Interactions Between Amino Acid-Tagged Naphthalenediimide and Single Walled Carbon Nanotubes for the Design and Construction of New Bioimaging Probes

*Zhiyuan Hu, G. Dan Pantoş, Navaratnarajah Kuganathan, Rory L. Arrowsmith, Robert M. J. Jacobs, Gabriele Kociok-Köhn, Justin O'Byrne, Kerstin Jurkschat, Pierre Burgos, Rex M. Tyrrell, Stan W. Botchway, Jeremy K. M. Sanders, and Sofia I. Pascu**

A new synthetic route to functionalized single walled carbon nanotubes (SWNTs) via supramolecular interactions using a specifically designed naphthalenediimide (NDI) nanoreceptor is demonstrated. The tendency of the NDI to spontaneously form composites with carbon nanomaterials leads to fluorescent amino acid tagged SWNTs, which are dispersible in widely accessible organic solvents ($CHCl_3$, DMSO) as well as in biocompatible cell medium (EMEM, Eagle's modified essential medium). The X-ray crystal structure of the first iodine-tagged and amino acid-functionalized NDI molecule, designed especially to facilitate the high resolution transmission electron microscopy (HR TEM) imaging whilst retaining its ability to self-assemble into a nanodimensional receptor in weakly polar solvents, is also described. A new hybrid material, NDI@SWNT, was prepared and characterized as dispersed in organic solvents and aqueous media and in the solid state by HR TEM, tapping mode atomic force microscopy (TM AFM), scanning electron microscopy (SEM), circular dichroism, Raman and fluorescence spectroscopies (steady-state single and two-photon techniques). Combined microscopy techniques, density functional theory (DFT) calculations using the Spanish Initiative for Electronic Simulations with Thousands of Atoms (SIESTA) program and spectroscopic measurements in solution indicate that amino acid-functionalized NDI interacts strongly with SWNTs and forms a donor-acceptor complex. Density functional theory (DFT) calculations predicted the geometry and the binding energies of an NDI molecule loaded onto a SWNT strand and the possibility of charge transfer interactions within the hybrid. The NDI@SWNT composite translocates into cells (e.g. FEK-4, HeLa, MCF-7) as an intact object and localizes in the cells' cytoplasm and partially in the nucleus. The NDI coating enhances the biocompatibility of SWNTs and mediates its intracellular localization as shown by confocal fluorescence imaging and fluorescence lifetime imaging (FLIM) techniques. The excited state fluorescence lifetime of the probes in cells versus solution phase indicates that the probes remain unaffected by the change in their chemical environment within the experimental timescale (2 h).

Z. Hu, Dr. G. D. Pantoş, R. L. Arrowsmith, Dr. G. Kociok-Köhn, J. O'Byrne, Dr. S. I. Pascu
Department of Chemistry
University of Bath
Claverton Down, BA2 7AY, UK
E-mail: s.pascu@bath.ac.uk
Prof. J. K. M. Sanders
Department of Chemistry
University of Cambridge
Lensfield Road, CB2 1EW, Cambridge,UK
Dr. R. M. J. Jacobs
Department of Chemistry
Chemistry Research Laboratory
University of Oxford
Mansfield Road, Oxford, OX1 3TA, UK

Prof. R. M. Tyrrell
Department of Pharmacy and Pharmacology
University of Bath
Claverton Down, BA2 7AY, UK
Dr. K. Jurkschat
Department of Materials
BegbrokeNano
University of Oxford, Oxford, UK
Dr. P. Burgos, Dr. S. W. Botchway
Central Laser Facility
Rutherford Appleton Laboratory, Research Complex at Harwell, STFC
Didcot, OX11 0QX, UK
Dr. N. Kuganathan
School of Chemistry
University of Nottingham
Nottingham, NG7 2RD UK

DOI: 10.1002/adfm.201101932

1. Introduction

New synthetic routes to functionalized fullerenes and carbon nanotubes using molecular recognition and encapsulation techniques can lead to optoelectronic materials with nanotechnological applications ranging from future photovoltaics[1,2] to nanoreactors for controlled chemical reactions[3] and to sensors and drug delivery devices.[4–8] Single walled carbon nanotubes have been studied for their potential as electronic nanodevices with unique electron transport properties on the nano-scale.[5,9] The supramolecular encapsulation of fluorescent molecules inside the hollow cavity of SWNTs (e.g. polythiophenes[10]) and their self-assembly onto the surface of aromatic carbon nanomaterials (e.g. tailor-made porphyrin hosts[11] or strong electron acceptors such as water solubile perylenes[12–14]) has been a lively area of exploration in the quest for new nanohybrids with potential applications ranging from new luminescent materials for solar cells[12,13] to molecular imaging tools.[5,6,8,9,13,15–36]

Naphthalenediimides (NDI) are emerging both as a building block for organic nanotube creation[37] and as a promising class of chromophores because of their strong absorption and fluorescence emission at visible and near IR wavelengths.[38] NDI fluorescence emissions show maxima between 300–800 nm, including in the spectral region where the interference from the autofluorescence of living cells may be bypassed; this makes them attractive candidates as building blocks for optical imaging probes.[38–45] NDI derivatives have been recently explored as DNA intercalators by virtue of their aromatic stacking with purines and pyrimidines[43,46,47] and as fluorescent tags for hypoxia-targeting probes such as nitroimidazoles.[48–50] Due to their aromatic stacking ability, fluorescence and electrochemical properties, NDIs are of interest as building blocks for biomimetic supramolecular and functional materials.[51–53] Amino acid-functionalized NDI molecules self-assemble into helical nanotubular, supramolecular structures from weakly polar solvents.[54,55] These dynamic structures are capable of recognizing and solubilizing fullerenes and ion pairs:[56] the Sanders group has shown that carbon materials such as C_{60} sense the helicity of the NDI host environment[57] whereas C_{70} provoked an entirely unexpected reorganization to give a hexameric receptor.[58] The NDI supramolecular nanotubes which have cavities with diameters in the range of 1–2 nm created by hydrogen bonding have been shown to act as receptors for aromatic molecules including naphthalene-based guests or fullerenes.[59,60]

Fluorescence imaging studies on fluorescent carbon nanotubes have thus far focused primarily on the measurement of the steady state spatial changes in emission intensity or wavelength.[4,15–19,21,23,61–68] The use of fluorescence lifetime imaging microscopy (FLIM) in combination with multiphoton excitation and near infrared (NIR) femtosecond laser pulses is widely used in the study of small molecule fluorophores particularly for in vitro studies.[69–72] To date FLIM has been used primarily on endogenous molecules such as tryptophan and common fluorescent dyes (e.g. GFP-tagged proteins and fluorescein-based derivatives),[73–75] with recent work exploring lifetime imaging of fluorescent platinum complexes permitting for the first time microsecond resolved emission imaging microscopy.[76] There are, to the best of our knowledge, thus far no reports on supramolecular assemblies involving carbon nanomaterials studied in cells by this method. The combination of two-photon excitation with fluorescence lifetime imaging techniques (FLIM) allows the use of near IR light to provide deeper tissue penetration, reduced cellular cytotoxicity and scattering and improved signal detection. Due to the defined nature of the emission lifetime and the sensitivity of lifetime measurements, excited state lifetime measurements could provide a powerful means by which to study donor-acceptor complexes in cells.

We have been interested in the design and spectroscopic investigation of new nanomaterials with light emitting properties.[67] The NDI nanotubular receptor recently developed[55] should have the ability to bind via donor–acceptor interactions to carbon nanomaterials, in an analogous manner to that found in the exciting new hybrids containing perylenes in SWNTs-electron acceptor composites for photovoltaic applications, reported by the groups of Hirsch[12–14] and Guldi.[14]

We report our investigations at the formation of a new nanohybrid, denoted NDI@SWNT, in solution and on a preparative scale. We report here for the first time, the recognition and coating of the aromatic surface of ultra-purified SWNTs (provided by Thomas Swan Ltd, Elicarb SWNTs, and further steam-puriffied to ensure they are free of catalytic impurities or carbonaceous materials from the nanotube synthesis, Supplementary Information) by a new iodine- and amino acid-derivatized NDI. Investigations into the properties of the new material synthesized (in bulk and in dispersions in $CHCl_3$, EtOH, DMSO and serum free aqueous cell culture media such as EMEM) have been carried out by Raman, circular dichroism, FT IR, UV–vis–NIR and fluorescence spectroscopies and imaged at the nanoscale by HR TEM, SEM, EDS and TM AFM. The cellular translocation of the resulting NDI@SWNT complex was investigated by a combination of fluorescence microscopy techniques including fluorescence lifetime imaging and cytotoxicity assays (MTT) in cancerous and non-cancerous cell lines. Here we have used such techniques to probe the integrity of a new nanocomposite denoted NDI@SWNT in vitro. Such an approach could aid the future understanding of the mechanism of action of supramolecular materials at the cellular level and improve the synthetic design of nanohybrids for biomedical imaging and therapeutic applications.

2. Results and Discussions

2.1. Synthesis and Single Crystal X-Ray Diffraction

The direct observation of these nanodimensional aggregates was carried out by electron microscopy techniques coupled with energy dispersive X-ray spectroscopy (EDS) analysis on modified NDI to include iodine (Z = 53) as a high scattering heavy element.

The new amino acid-derivatized and iodine-tagged NDI was synthesized from L-4-iodophenylalanine and 1,4,5,8-naphtalene-tetracarboxylic dianhydride, using a microwave-assisted method.[54,55] The molecular structure and supramolecular architecture of NDI was determined in the solid state by single crystal X-ray crystallography (**Figure 1**). The NDI molecules are

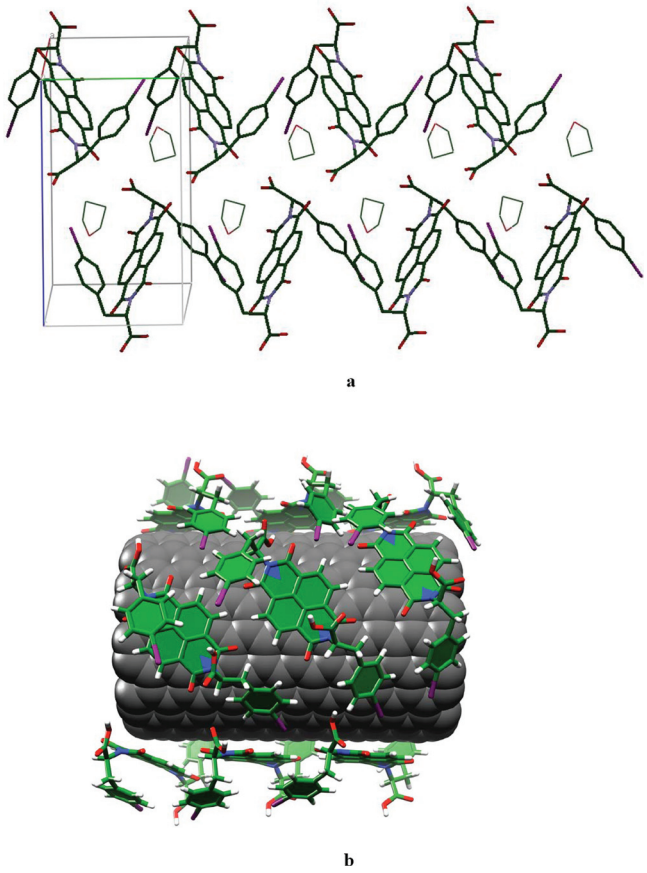

Figure 1. a) X-ray structure of NDI: unit cell fragment, view over axis *a*; b) Proposed structure of a fragment of NDI@SWNT composite: molecular mechanics minimized representation (MM+, Forcite, Material Studio) of NDI stacks self-assembled on the surface of a [10:10] SWNT fragment.

oriented face-on and show two amino acid groups placed *anti* with respect to the aromatic core. No aromatic stacking was observed in the unit cell but intramolecular and intermolecular dipole interactions link up stacks of NDI molecules, whereby the I···(O)COH dipole interactions have rather short (3.184 Å) separations. Thus, the NDI supramolecular structure shows weakly linked (hence flexible and likely to act as adaptive materials) tubular arrangements in the solid state, with cavities of circa 1.24 nm filled with disordered crystallizing solvents.

To isolate NDI@SWNT on a preparative scale, a solution of NDI dissolved in $CHCl_3$:EtOH 4:1 (6 mg/mL) was treated with 1 mg of pristine, steam-purified single walled carbon nanotubes (Elicarb, Thomas Swann Ltd, Supplementary Information). The mixture was sonicated for 30 min (340 W), followed by centrifugation (1500 rotations/min) and filtration (a 200 nm pore diameter membrane). The separated solid material was dispersed in minimum amount of $CHCl_3$:EtOH 4:1 and the sonication, centrifugation and filtration sequence was repeated at least 3 times (*stages 1-3* of dispersion experiment). Liquid phases were analyzed by UV–vis, UV–vis–NIR and steady state fluorescence spectroscopies, which confirmed the removal of excess and weakly bound NDI and the presence of dispersible SWNTs. After at least 3 cycles of dispersion/filtration, the resulting solid residue denoted NDI@SWNT was redispersed in $CHCl_3$:EtOH 4:1 (with 30 min sonication, *stage 4*) to give a transparent dispersion (0.2 mg/mL, Supplementary Information) which was stable for days without precipitation. Formation of stable and clear dispersions was also observed when DMSO or aqueous cell medium (EMEM, Eagle's modified essential medium, phenol-red free) were used to 'solubilise' the NDI@SWNT hybrid.

2.2. Molecular Modeling

In an attempt to describe the structure of NDI@SWNT, we propose a molecular mechanics (MM+, Forcite) model of SWNT encapsulated within the supramolecular nanotubular receptor framework of NDI based on the X-ray structure determination of the NDI (Figure 1). It has already been shown that certain NDI networks may adjust their adaptable tubular cavities in order to encapsulate via aromatic stacking guests with diameters in the range of 1 nm (for C_{60}[57] or C_{70}[58]). DFT computational modeling was used to aid our understanding of the geometry adopted by an isolated NDI molecule in the presence of a SWNT and the nature of its interactions with this aromatic guest. Here, the simplified SWNT model used was 1.6 nm wide. A hierarchy of DFT-based codes (SIESTA, Spanish Initiative for Electronic Simulations with Thousands of Atoms[77]) allowed the ab initio total energy calculations of these large systems, thus aiding investigations of the structural and electronic behavior of NDI absorbed onto SWNTs (**Figure 2** and Supplementary Information). To examine more closely the interaction between an isolated NDI molecule and SWNT surface we modelled at the DFT level a simplified capped model

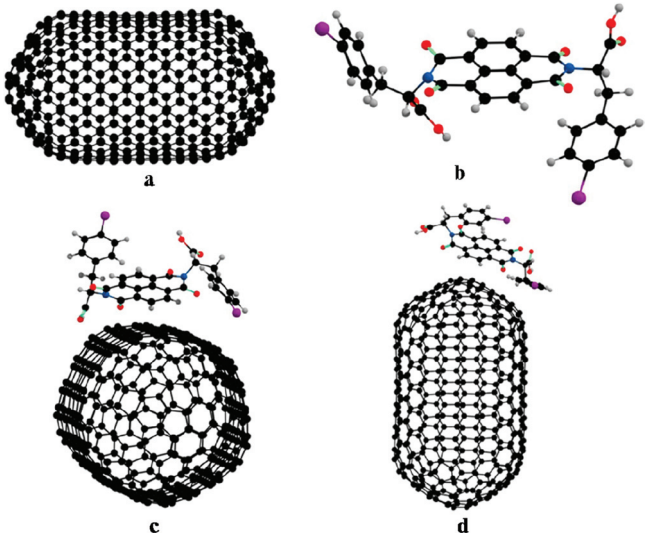

Figure 2. DFT-level optimized geometries (SIESTA) of model compounds: (a) a short [10,10] capped SWNT; (b) NDI molecule; (c) NDI molecule bound supramolecularly onto the middle part of a [10,10] capped SWNT (geometry A); (d) NDI molecule bound to the tip of a [10,10] capped SWNT (geometry B).

Table 1. DFT-calculated binding energies E_b(eV) and NDI-aromatic guest distances in the optimised composite geometries. For a comparison, the gas-phase DFT estimated charge transfer at the absorbtion of NDI onto C_{60} (NDI:SWNT 1:1) is also given.

System	Charge transfer [NDI/aromatic surface]	Closest C-C distances between aromatic surface and NDI (Å)	Uncorrected binding energy (eV) E_b (unc) [a)]	Corrected binding energy (eV) $E_{b\ (CP)}$ [b)]
NDI@C_{60}	0.024	3.230, 3.294, 3.307, 3.334, 3.462, 3.484, 3.523	–0.66	–0.31
NDI@SWNT (Configuration A, middle of SWNT)	0.086	3.150, 3.310, 3.455, 3.700, 4.020, 4.090, 4.140	–1.03	–0.84
NDI@SWNT (Configuration B, tip of SWNT)	0.044	2.926, 3.104, 3.360, 3.398, 3.587, 3.853, 3.920	–0.95	–0.66

Note: [a)]Defined as described in Supplementary Information; [b)]Determined by the counterpoise correction (CP) method.[108]

of a short [10,10] SWNT and two possible geometries (**A** and **B**, Figures 2c and 2d, respectively) for the corresponding NDI:SWNT 1:1 complex.
Geometry A) NDI decorates the sidewall of the SWNT *and*
Geometry B) NDI is bound *face-on* to the tip of the SWNT.

Table 1 shows calculated distances at the binding of NDI to SWNTs. These compare well with the known, simpler model of NDI molecule bound to C_{60}. The calculated binding energies for the NDI interaction with the sidewall of the SWNT and to the tip of the SWNT are –0.84 eV and –0.66 eV respectively, indicating a π-orbital interaction between the NDI aromatic ring and the aromatic network of the model SWNT. According to the DFT estimated binding energies (Table 1 and Supplementary materials), it is clear that the interaction between NDI and SWNT is of a similar order of magnitude to that between NDI and C_{60} and these are both of a rather weak non-covalent nature. In terms of binding energy values the NDI molecule binds more strongly to a singe strand of a short and idealized [10,10] SWNT than to a C_{60} molecule. One of the limitations in the DFT model used is the overestimation of the binding energy caused by weak interactions.[78] This has been first highlighted for the modelling of a supramolecular benzene dimer.[79,78] For this simple aromatic stacking model interaction DFT calculations yielded an inter-ring distance of 3.06 Å and a binding energy of –0.48 eV, whereas higher level modelling (CCSD (T)) calculations gave corresponding values of 4.1 Å and –0.05 eV respectively.[79] A similar computational approach was applied hereby (see Supporting Information), and was detailed in a previous publication.[67]

Calculations showed that for a model NDI@SWNT composite with geometry **A** (Figure 2c, where an NDI molecule is bound to the middle of the SWNT strand, ca. 0.086 electrons were transferred between a molecule of NDI and the [10, 10] SWNT. For the NDI@SWNT composite in the tip-binding geometry **B** (Figure 2d), 0.044 electrons were transferred between NDI and the carbon nanotube. In order to investigate the charge transfer between two adjacent NDI molecules we performed a control calculation in the absence of SWNT, where only two stacked NDI molecules modeled. Initial geometries for the NDI–NDI complex were generated using a fragment of the asymmetric unit for the X-ray structure determination. This showed that a negligible NDI-NDI charge transfer occurs in the absence of the aromatic guest (C_{60} or SWNT).

Our DFT-optimized model used for computational studies considered only a very short length for the SWNT modeled (200 nm): this allows maximum 6 NDI molecules to bind in configuration **A** (to the middle part of the SWNT) and a further 4 NDI molecules to bind in configuration **B** (coating the tip of the SWNTs). According to gas-phase DFT modeling, NDI and SWNTs are held together by non-covalent interactions whereby approximately 2 electrons are transferred between the nanoreceptor formed by 10 molecules of NDI absorbed onto the outer surface of a 500 nm long capped SWNT fragment. In solution, steady-state fluorescence spectroscopy showed a significant quenching of NDI emission in the presence of SWNTs. DFT calculations support the hypothesis that donor-acceptor interactions may occur between NDI and SWNTs and that these are similar in nature to those found in known NDI-C_{60} complexes.[57]

2.3. Spectroscopic Investigations on the NDI@SWNT Composite

Solid state FT-IR spectroscopy (Supplementary Information) of the solid composite prepared as above suggested functionalization associated with nanotubes, with the spectrum clearly showing the carbonyl (C=O) stretching at 1730 cm^{-1}, C–O stretching at 1100 cm^{-1} and O–H band at 3300 cm^{-1}. Thus the presence of carboxylic groups associated with the tubes due to the amino acid tagged NDI was confirmed.

Raman spectroscopy is a powerful tool for characterizing functionalized carbon nanomaterials:[80,81] spectra shown in were recorded for dispersed samples deposited from $CHCl_3$:EtOH (4:1) or DMSO using λ_{ex} = 830 nm, i.e. a region of the emission spectra of the NDI@SWNT without interference from fluorescence emission from NDI. NDI@SWNT showed features consistent with the occurrence of defects in the tube surface post-functionalization with respect to free SWNTs. The G band (which corresponds to a splitting of the E2g stretching mode of graphite and reflects the structural intensity of the sp^2-hybridized carbon atoms) at ~1590 cm^{-1} and a disordered D band (generally attributed to the disordered graphite structure of the nanotubes) at ~1330 cm^{-1} were observed. For dried samples, deposited from $CHCl_3$:EtOH 4:1, an increase in the I_D/I_G band intensity ratio of the NDI@SWNT solid composite (15%) was observed compared to the I_D/I_G of free SWNTs

(9.5%), confirming that the supramolecular functionalization of SWNTs has occurred (**Figure 4**).[82,83]

Raman spectra of NDI@SWNT also showed a G' band at ca. 2600 cm^{-1} as well as the radial breathing modes (RBM) between 140–300 cm^{-1}. The latter signal remained largely unchanged with respect to that of the starting material steam-purified SWNTs in DMSO or EMEM. Several broad peaks centered at 150, 165, 189, 235, 239, and 270 cm^{-1} are observed for pristine SWNTs samples and are also visible in the spectra of NDI@SWNT particles deposited on borosilicate glass slides from all solvents investigated, i.e. $CHCl_3$:EtOH 4:1, DMSO and aqueous media EMEM). The pure SWNT sample contains tubes with a broad diameter ranging between 1.8 and 0.8 nm. RBM maxima indicate that tubes with diameters of 1.6, 1, and 0.86 nm are mainly present (Supporting Information) in the starting material used. The spectrum of NDI@SWNT showed significant enhancement and sharpening of the RMB peaks at 147.5, 165 and 240 cm^{-1} respectively, with respect to the RBMs of the pristine SWNTs used. This indicates that in $CHCl_3$:EtOH 4:1, NDI@SWNTs dispersions contain tubes with diameters of 1.65, 1.47, 0.93 nm (Figure 4).

To determine the most reliable NDI:SWNT mass ratio likely to lead to a complete binding of NDI to SWNT and stable dispersions (with respect to nanoparticle precipitation over 24 h) in common solvents, fluorescence and UV–vis spectroscopic titrations of NDI solutions onto SWNTs dispersions were carried out in several common solvents ($CHCl_3$, EtOH, DMSO) (**Figure 3**). First, aliquots of 2 μg/mL of NDI were added followed by 5 minutes sonication prior to recording each spectrum. The optimum NDI: SWNT mass ratio was obtained when a solution of 26 μM of NDI (21 μg/mL) was anchored onto 35 μg/ml SWNTs dispersed in $CHCl_3$: EtOH 4:1, DMSO or aqueous medium EMEM (containing up to 5% DMSO) giving the NDI: SWNT mass ratio 0.6. secondly, the titration experiment was also repeated by the addition of SWNTs (dispersed in $CHCl_3$:EtOH, 20 μg/mL aliquots) to a solution of NDI (26 μM). The direct spectroscopic observation for the SWNT surface recognition by NDI was thus achieved: NDI@SWNT formation on a preparative scale (using excess of NDI and the filtration/redispersion procedure described above) as well as titration experiments showed an extremely rapid quenching (with ca. 80% decrease in fluorescence intensity) of the NDI fluorescence emission in the presence of SWNTs. Titration curves obtained were typical of very strong binding, as shown in ESI. The binding of NDI to SWNTs appears to be too tight in solution and did not allow an accurate determination of the association constant using standard binding isotherms.[84] Similar binding curves with extremely sharp end-points were recently observed at the tight noncovalent binding of porphyrin oligomers to SWNTs: the binding constant was believed to be higher than 10^7 M^{-1} in such cases.[84]

The UV–vis spectroscopy of NDI@SWNT recorded in aqueous medium (EMEM) or in organic solvents $CHCl_3$, $CHCl_3$/EtOH, DMSO and EtOH showed very similar features (Figure 3). UV–vis spectroscopy showed that both NDI@SWNT and free dye NDI have broad and complex excitation spectra with three characteristic maxima in the 300-400 nm region. The occurrence of a new band was observed in the UV–vis spectra of samples containing SWNTs (λ_{max} = 280 nm), as well as significant broadening and red-shifting of the bands in the 388 nm region. In DMSO or in aqueous cells media (EMEM containing 1% DMSO), NDI@SWNT dispersions showed a ca. 6 nm red-shift of the band at 388 nm compared with the organic solvents investigated ($CHCl_3$, EtOH). This suggests that the interaction between SWNTs and the NDI molecules absorbed is stronger in biocompatible environment (the cell culture media EMEM or in DMSO) than in the standard organic solvents investigated ($CHCl_3$, EtOH).

The fluorescence spectra of NDI@SWNTs were recorded for excitation wavelengths between 200 and 800 nm in $CHCl_3$:EtOH, DMSO or aqueous media (EMEM, of relevance for bioimaging investigations) and are broader than those of the free NDI. Both NDI and NDI@SWNT show two emission maxima in the range 300–700 nm (Supporting Information). The position of these bands seems strongly influenced by the nature of the solvent and concentration. As stated above, the severe quenching of the fluorescence emission intensity was observed after adding SWNT (Figure 3c), indicating the strong absorption of the aromatic coating material onto the surface of the nanotube.[44] A red-shift in the emission maxima of NDI (20 nm) was also observed upon its anchoring onto SWNTs (Supplementary materials). The broadening in the UV–vis spectra as well as decay in the fluorescence emission intensity with time was observed, and this behavior stabilizes after 24 h presumably as the NDI absorption onto SWNTs reaches completion. The presence of the SWNT as the aromatic "guest" within the NDI supramolecular network (which acts as a "nanoreceptor") makes the dispersion phase determination of the fluorescence quantum yield of NDI@SWNT difficult to ascertain with precision. The quantum yield of the free dye was estimated as 2.4% in $CHCl_3$ and 1.6% in EtOH (relative to $[Ru(bipy)_3][PF_6]_2$ in H_2O,[85] which is within the range expected for this class of compounds.[86]

The circular dichroism (CD) spectrum at the free NDI absorbance (330–400 nm) was assigned to interactions between the NDI couplets of sequential interacting NDI chromophores.[87] Changes in the relative position of these moieties lead to changes in the CD fingerprint of the supramolecular assembly. CD spectroscopy showed new features for the NDI@SWNT composite which are due to NDI upon absorption onto the carbon nanomaterial, i.e., the sequential interacting NDIs change their relative position, leading to changes in the 380 nm region of circular dichroism spectrum and the appearance of a new signal in the 260–280 nm region (Figure 3b). CD spectroscopy shows that the initial aggregation motif of free NDI in solution is being altered by the presence of SWNT. The chirality of the amino acid-derivatized NDI molecule is also observed in the NDI@SWNT composites: this is consistent with earlier reports on DNA@SWNT composites studied by this method, whereby DNA helicity was believed to be sensed by carbon nanotubes in dispersions.[22,88,89]

The UV–vis–NIR spectra of NDI@SWNT (recorded in pure $CHCl_3$ or mixtures of $CHCl_3$:EtOH 4:1) shows the lowest-energy van Hove transition S_{11} for NDI@SWNT (at 1204 nm), and also typical S_{22} transitions at in the 960 nm region (Figure 3f). Partially overlapping of S_{22} and metallic M_{11} transitions characteristic to SWNTs can be seen at 500-1000 nm in NDI@SWNT dispersions. The S_{22} and S_{11} band are sharp compared

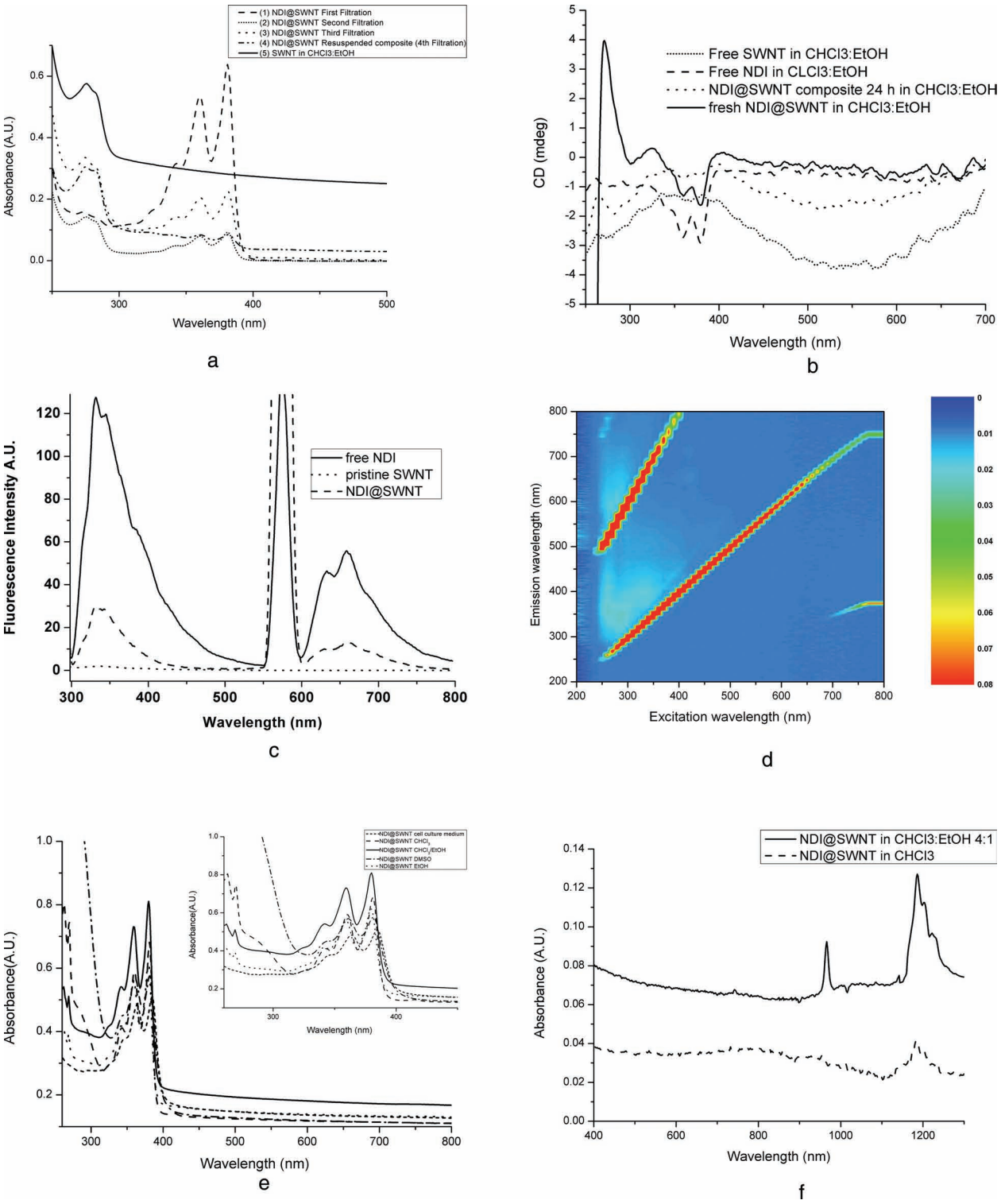

Figure 3. a) Preparation of NDI@SWNT monitored by UV–vis spectroscopy in CHCl3:EtOH 4:1. *(1)-(3):* NDI@SWNTs composites during the *stages 1-3* of the synthetic experiment; *(4):* redispersed NDI@SWNT composite from *stage 4* (0.2 mg/ml) and *(5):* free SWNT (0.35 mg/mL); b) CD spectra of NDI@SWNT composite, recorded in fresh dispersions (20 min, followed by filtration through a 200 nm pore PTFE membrane) or after storing at r.t. for 24 h (0.2 mg/mL, $CHCl_3$:EtOH 4:1); c) Typical fluorescence emission spectra showing the NDI fluorescence quenching upon treatment of a diluted solution of NDI (26 μM in $CHCl_3$:EtOH 4:1, λ_{ex} = 280 nm) with SWNT (35 μg/mL); d) Emission/excitation map (normalised intensity) showing that the redispersed NDI@SWNT composite resulting after the *stage 4* of the redispersion experiment retains fluorescence (0.2 mg/mL $CHCl_3$:EtOH 4:1). e) UV–vis spectroscopy of NDI@SWNT (0.2 mg/mL) in organic and in aqueous cell culture media (EMEM). f) UV–vis–nIR spectroscopy of NDI@SWNT composite (0.2 mg/mL, $CHCl_3$:EtOH 4:1 and pure $CHCl_3$ dispersions).

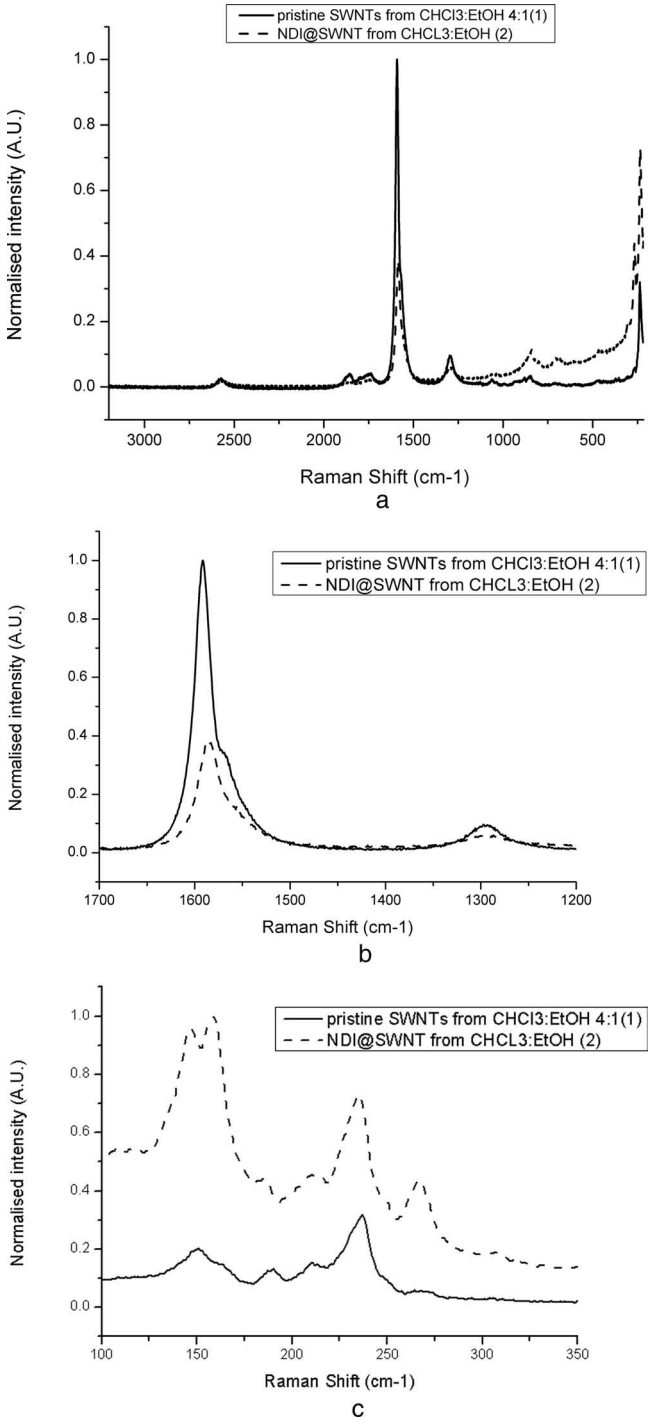

Figure 4. Raman spectroscopy of purified SWNT and NDI-functionalized SWNTs (λ_{ex} 830 nm, laser power at the sample 220 mW spot size 100 μm. a) Full spectra for materials deposited on borosilicate glass from $CHCl_3$:EtOH 4:1, 0.2 mg/mL dispersions; b) expansion diagnostic of surface fuctionalization of SWNT, showing D and G bands for $CHCl_3$:EtOH 4:1. c) RBM of SWNT upon NDI complexation. Spectra of solid materials were recorded at least three times from different areas of the nanomaterial and the average spectra reported.

to those observed in other supramolecularly functionalized SWNT composites (for example those of peptides[82,90,91] or porphyrin oligomers[84]) absorbed onto the SWNTs, and closely similar to those observed in perylene-SWNTs composites.[12,13] Since these transition energies are related to the size of the SWNT bundles and the presence of isolated tubes in solution have been reported to give rise to sharp, well-resolved peaks,[29] UV–vis–nIR spectroscopy of the NDI@SWNT composite suggests that NDI is capable of efficient de-bundling of the SWNT strands in these common solvents.

2.4. Microscopy Studies on NDI@SWNT by HR TEM, AFM and SEM

High resolution transmission microscopy (HR TEM, Jeol 3000F) provided direct evidence for the presence of a monolayer of NDI coating the walls of the SWNTs (**Figure 5**). Areas of strong contrast due to heavy elements, attributable to iodine atoms, are clearly visible with respect to the lighter regions (due to the lower scattering elements present, i.e. carbon, hydrogen, nitrogen, oxygen) and in contrast to the initially clean SWNT surface observed for the high purity SWNTs used (Supplementary Information). HR TEM also showed that NDI coated the ends of the SWNTs and that the NDI layer is less than 2 nm thick, consistent with the qualitative molecular mechanics model proposed in Figure 1 for a NDI-wrapped single strand of a [10,10] SWNT. The presence of amorphous carbon created by beam damage of the soft coating under the HRTEM working conditions cannot be fully discounted, but both low resolution TEM and HR TEM coupled with EDX allowed us to probe locally the surface of nanotubes where such dark spots were observed (Figure 5a). Characteristic peaks corresponding to iodine were detected in the EDX spectra in the 4 keV region. By contrast with the large bundles typically observed for purified but unfunctionalized SWNT starting material the NDI coated nanotubes tended to aggregate into much smaller bundles or form only single strands in polar solvents. The morphology of these new aggregates was confirmed by SEM and tapping mode AFM (TM AFM) (**Figure 6**). The coating with NDI was uniform and covered the entire aromatic surface of SWNTs. TM AFM of free NDI (spin-coated on mica surfaces from 0.2 mg/mL solutions in $CHCl_3$:EtOH 4:1) showed formation of tower-like aggregates with heights of ca. 10 nm and diameters of ca. 2 nm. TM AFM of the NDI@SWNT composite (spin-coated on a mica surface from the ca. 0.2 mg/mL dispersion in $CHCl_3$:EtOH) confirmed the complete coating of the SWNTs and formation of small NDI@SWNT bundles with lengths of ca. 500 nm, and heights ranging from 10-50 nm, without free (unbound) NDI aggregates on the mica surface.

2.5. Multiphoton Fluorescence Imaging in Solution and in Vitro

To probe the potential of NDI@SWNT as a precursor for future applications as traceable imaging probes inside living cells, two-photon emission lifetime decay spectra were recorded by time-correlated single photon counting using pulsed laser excitation (λ_{ex} = 910 nm in DMSO). DMSO was chosen as both NDI and NDI@SWNT showed minimum scattering due to aggregation within the experimental timescale in this solvent and due to its low volatility. Both systems exhibited more than one lifetime

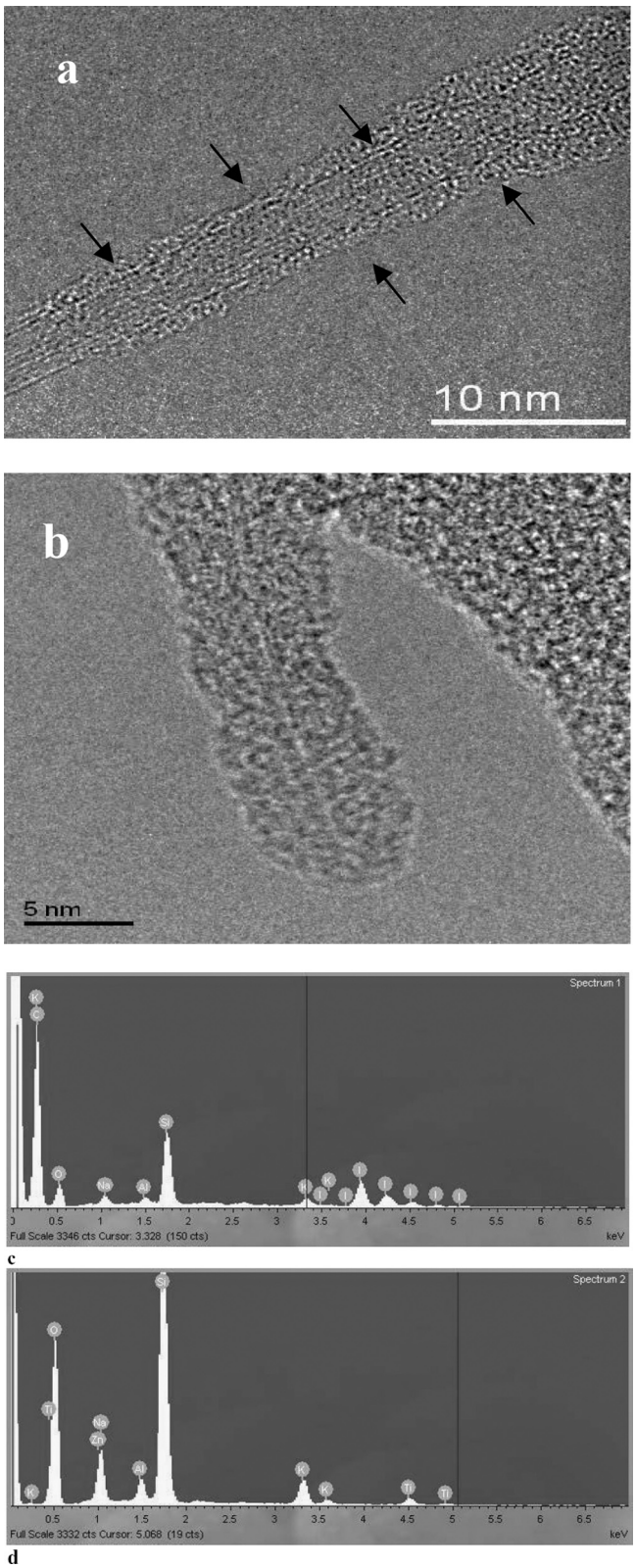

Figure 5. a,b) Representative images from HR TEM of NDI@SWNT composite showing the presence of iodine in local areas of strong contrast due to the heavy element on the surface of nanotubes (marked with arrows in Figure (a)). c) The EDS spectrum of NDI@SWNT composite deposited on glass support and d) control EDS spectrum.

component: calculations (SPC Image analysis software) indicated a long component on the order of several nanoseconds and a much shorter component on the order of several hundred picoseconds. There are several differences between the lifetime decay spectra profiles of free NDI and NDI@SWNT (**Figure 7**), i.e., the lifetime of the long component drops by ca. 10%, from 2.67 ns (36% weighting) in free NDI to 2.33 ns (27% weighting) in NDI@SWNT. Only a slight increase in the short component lifetime weighting was found for the dominant component, from (0.43 ns) 64% weighting in free NDI 73% weighting for NDI@SWNT dispersions. The decrease in fluorescence lifetime of NDI upon immobilization onto the SWNT (in DMSO) confirmed the fluorescence quenching by the SWNT surface via non-radiative pathways, in agreement with earlier reports on polythiophene-SWNTs nanohybrids.[26]

For the high resolution laser scanning confocal fluorescence imaging of NDI@SWNT fresh dispersions (0.2 mg/mL in $CHCl_3$:EtOH 4:1) were dropcast on a borosilicate glass cover slip and the solvent evaporated under air. High-resolution confocal imaging under single-photon (488 nm) or two-photon excitation (910 nm), using a mode-locked Ti-sapphire laser (see Supplementary Information), generated images of the solid NDI@SWNT film by the raster scanning of the laser spot in the *xy* plane. Two photon fluorescence imaging and emission lifetime measurements were carried out, using FLIM in solid state composite (deposited on borosilicate glass from $CHCl_3$:EtOH 4:1 dispersions) and in HeLa and MCF-7 cell lines (vide infra) for NDI and NDI@SWNT. Single photon laser scanning confocal fluorescence imaging carried out in the absence of cells showed that the film of solid NDI@SWNT particles retains some residual fluorescence emission under single photon excitation (λ_{ex} 488 nm) but this composite is a rather weak fluorophore with respect to standard organic dyes. Within the NDI@SWNT film (**Figure 8**), fluorescent aggregates with irregular shapes and sizes ranging from ca. 200 nm to 5 μm were observed in the differential interference contrast (DIC) microscopy images, in the red (λ_{em} = 606 nm) and green (λ_{em} = 516 nm) channels of the single photon fluorescence emission images (λ_{ex} 488 nm), as well as by two-photon fluorescence intensity and lifetime imaging (λ_{ex} 910 nm). Intensity images of NDI@SWNT obtained from two-photon fluorescence excitation gave better signal to noise than one-photon excitation and fluorescence lifetime imaging and corresponding data fitting was obtained when 2-photon FLIM measurements were used. The preliminary fluorescence lifetime imaging shows lifetime emission maps for NDI@SWNT together with intensity maps showing the spatial variations in fluorescence emission and the lifetime distribution plots for the major lifetime component. For NDI@SWNT, the maximum fluorescence lifetime in the solid state of the major component (0.42 ns, with width at half-height WHH of +/–0.12 ns) is similar to the fluorescence lifetime measured in pure DMSO solution for (0.41 ns).

To test the biocompatibility and in vitro stability of the NDI@SWNT composite, cancerous (breast carcinoma MCF-7 and cervical carcinoma HeLa) and healthy (fibroblast FEK-4) cells were treated with the composite dispersed in cell medium EMEM over a range of concentrations. Despite the strong quenching observed with respect to the free NDI fluorescence emission, some residual emission of the NDI absorbed onto SWNTs was

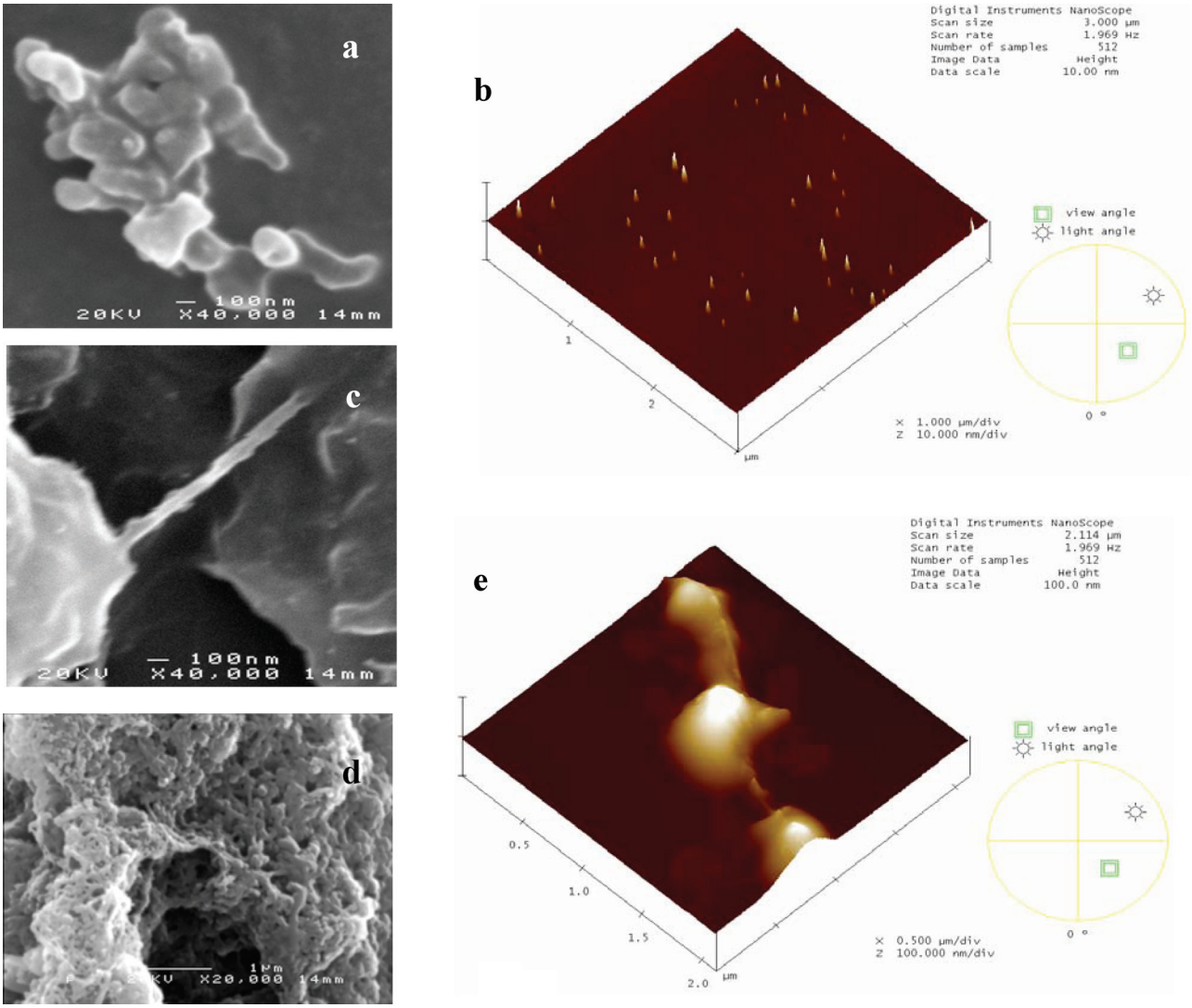

Figure 6. SEM and TM AFM imaging of NDI and NDI@SWNT deposited from CHCl3:EtOH,. Aggregates of free NDI formed upon spin-coating onto a mica substrate, imaged by SEM (a) and TM AFM (b) showing formation of nanodimensional tower-like objects on mica; SEM microscopy images showing a small bundle of NDI-coated SWNTs (c) and the morphology of NDI@SWNT (d); TM AFM imaging of NDI@SWNT (e). All SEM measurements were carried out on samples coated with ca. 2 nm gold layer. Concentrations: free NDI 26 µM; NDI@SWNT composite dispersion containing 21 µg/mL NDI (26 µM) anchored onto 35 µg/mL SWNT.

sufficient to enable the observation of the nanocomposite in living cells (**Figure 9** and **Figure 10** and Supplementary Information, S10, S12b, S13b, S14e-h and S15a-d). Cell uptake was monitored in living cells by epi-fluorescence microscopy (following 30 min, 2 h, 3h or 5h incubation with NDI@SWNTs at 4 °C and 37 °C, λ_{ex} 450 nm) and by single-photon laser scanning confocal fluorescence imaging (λ_{ex} = 488 nm, 30 min, 1 h and 2 h incubation at 37 °C, Figure 9). The composites penetrate cell membranes at 37 °C but not at 4 °C, suggesting active uptake, possibly endocytosis, as the likely uptake mechanism.[22] Confocal imaging using λ_{ex} 405 nm did not show fluorescence emission for either free NDI or NDI@SWNT composite and therefore suitable images staining with Hoechst or DAPI nuclear staining (Invitrogen) were acquired (Figure S15). Colocalisation experiments showed some nuclear uptake for free NDI in all cell lines and this seems to increase in cells after 1 h incubation, as indicated by co-staining with Hoechst nuclear stain and fluorescence lifetime imaging (vide infra).

To verify whether the supramolecular NDI@SWNT composite remains stable in vitro with respect to NDI loss, fluorescence emission lifetime measurements were carried out using 2-photon FLIM in HeLa or MCF-7 cell lines (1 h incubation, 37 °C, using 910 nm excitation from a mode locked Mira titanium sapphire laser, 180 fs pulse, 75 MHz) and data was compared with FLIM of the free NDI under identical conditions. Similar to the case of FLIM of the solid NDI@SWNT composite, data fitting for FLIM measurements of NDI@SWNT in cells was significantly more reliable for 2-photon excitation than compared to the 1-photon measurements. Figure 10d–h shows lifetime emission maps for NDI and NDI@SWNT in HeLa cells

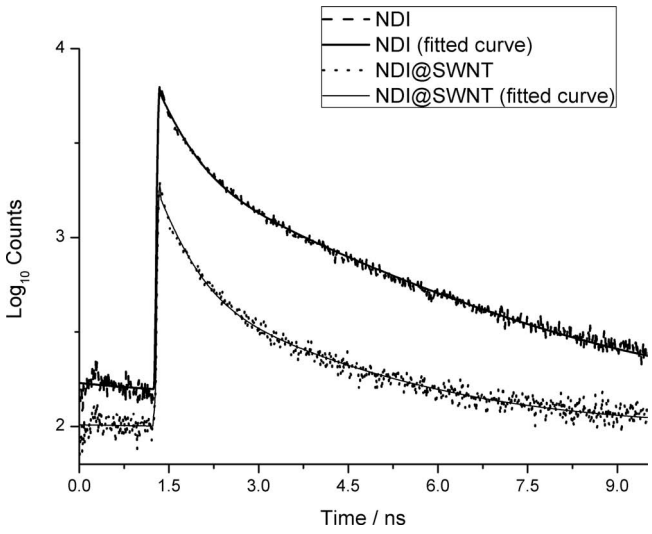

Figure 7. Two-photon fluorescence spectroscopy: fluorescence decay traces and corresponding fitted curves for the lifetime determinations (λ_{ex} = 910 nm, NDI 26 μM, pure DMSO, NDI@SWNT composite dispersion containing 21 μg/mL NDI (26 μM) anchored onto 35 μg/mL SWNT).

together with 2-photon intensity maps showing the spatial variations in fluorescence emission, the lifetime imaging maps and corresponding distribution plots for the predominant lifetime component (τ_1) for either free NDI or NDI@SWNT composite. Similar images are included in Supplementary materials for the FLIM of NDI and NDI@SWNT in the MCF-7 cell line. The lifetimes distributions measured inside cells are within the same order of magnitude with the values acquired from studies in pure DMSO (Figure 7) for both the NDI and the NDI@SWNTs and compare well with the FLIM of the solid NDI@SWNT. The major lifetime components measured in cells incubated for 1 hour (37 °C) were 0.65 ± 0.15 ns for free NDI inside cells and 1.10 ± 0.10 ns for NDI@SWNT in HeLa. A much broader lifetime distribution inside the cells than in solution or solid state was observed, and images of NDI@SWNT in HeLa cells showed regions of extremely high fluorescence intensity, corresponding to particles of ca 4 μm with extremely short emission lifetimes by 2-photon FLIM (0.07 ns or less). As expected, the relative weightings of the lifetime components obtained were somewhat different under the different conditions employed for cellular *vs.* solution lifetime estimations.[76] An inspection of the DIC and confocal images suggest that these large aggregates contain SWNTs coated in fluorescent materials and are concentrated in the proximity of the cell membrane and also bound on the outer surface of the cell. Initial tests on the co-localisation of NDI and NDI@SWNT with the mitochondrial stains Mitotracker Red, and lysosome stain Lysotracker Red (Invitrogen) were carried out but results did not show any conclusive mitochondrial or lysosomal colocalisation. There was evident nuclear uptake both in the HeLa and in FEK-4 cell lines and this seems to increase in cells after 2 h incubation, as indicated by co-staining with Hoechst and fluorescence lifetime imaging. Further colocalisation tests using alternative stains to fully identify the specific sites of cellular localisation for these compounds and their effect on the cellular organelles are underway.

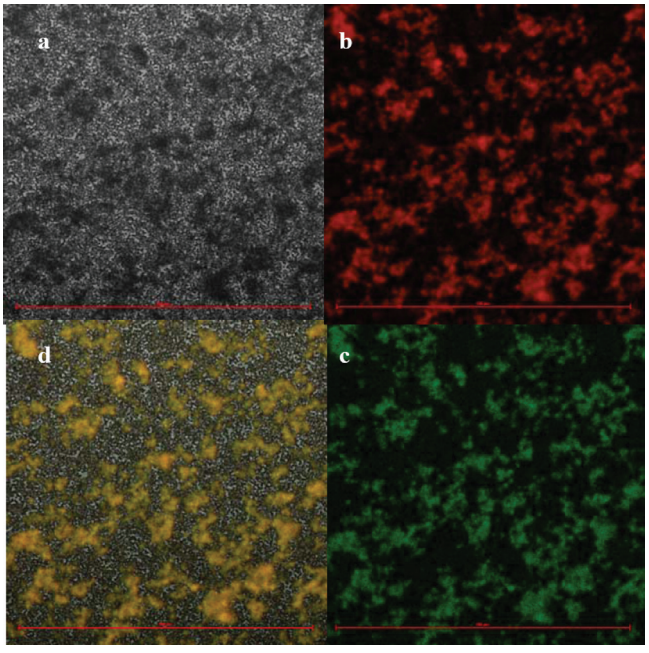

Figure 8. Single photon confocal imaging (scale-bar 100 μm, λ_{ex} = 488 nm) of solid NDI@SWNT composite drop-cast on borosilicate glass from a $CHCl_3$:EtOH 4:1 mixture showing: a) brightfield microscopy image b) red channel emission (606 nm); c) green channel emission (516 nm) and d) overlay of (a)–(c) microscopy images.

2.6. Cellular Translocation Monitoring of NDI@SWNT by MTT Assays

The different spatial distributions observed by DIC imaging coupled with fluorescence imaging and FLIM for the free NDI and NDI@SWNT in vitro suggests that the nanocomposite translocates into cells as a distinct intact entity and remains largely intact in the cellular environment within the timescale of these imaging experiments, i.e., is kinetically stable with respect to de-complexation by loss of NDI in vitro within the timescale of this experiment. Since the naphthalene diimines and structurally related monoimides are known to show cell toxicity and potent antitumor activities by virtue of their DNA binding[41,92] standard MTT assays were used here to verify the cell viability in the presence of NDI, SWNT and NDI@SWNT under conditions similar to those used in the fluorescence microscopy studies (Supplementary Materials). Assays showed that the materials investigated (free SWNTs, free NDI and NDI@SWNT hybrid) had only a moderate impact on cell viability at the 1 h time point at the same concentration used in the fluorescence studies. In separate experiments, cell metabolism MI_{50} values (the concentration that reduces cell metabolism to half that of untreated cells) were also determined via MTT assays over the traditional 24 h period. Dispersions of NDI, NDI@SWNT and free SWNT (1% DMSO in Eagle's Modified essential medium EMEM containing 15% foetal calf serum FCS) were incubated with HeLa cells for 24 h at concentrations of 1 nM, 100 nM, 1 μM, 10 μM, 50 μM, 100 μM and 250 μM for NDI or NDI-anchored

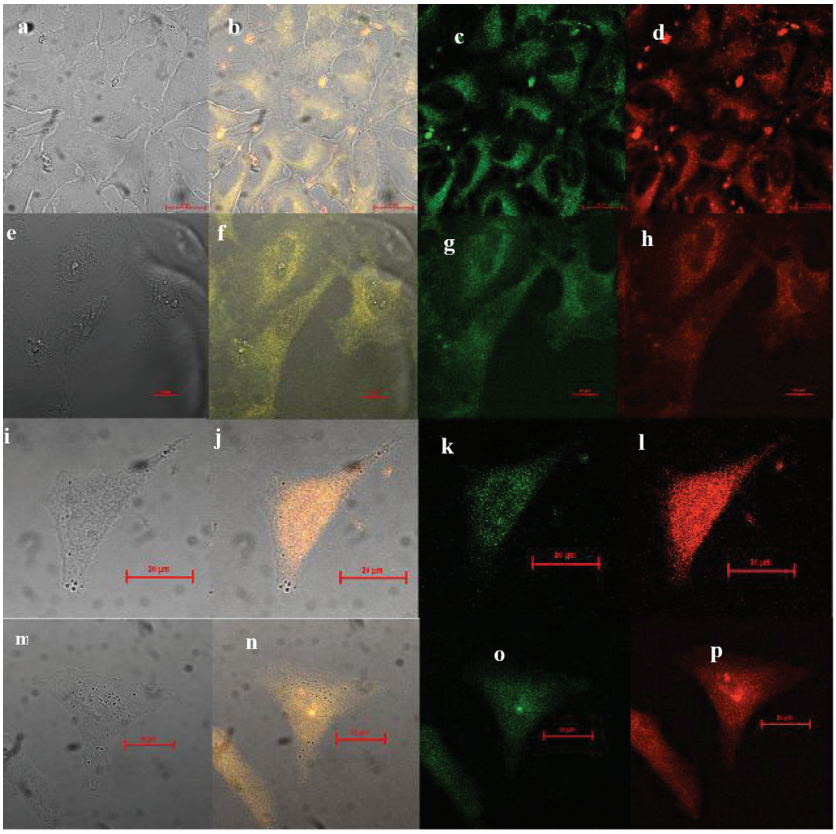

Figure 9. Single Photon Laser scanning confocal imaging of cancerous (HeLa) cells incubated at 37 °C where λ_{ex} = 488 nm with: a–l) NDI imaging (26 μM or 21 μg/mL in 1: 99% DMSO:EMEM) – 30 min incubation showing DIC (a), DIC-green-red channel overlay (b), green channel (515-530 nm) (c) and red channel (605-675 nm) (d); e–h) 1 h incubation showing DIC (e), DIC-green-red channels overlay (f), green channel (515-530 nm) (g) and red channel (605–675 nm) (h); i–l) 2 h incubation showing DIC (i), DIC-green-red channels overlay (j), green channel (515-530 nm) (k) and red channels (605-675 nm) (l); (m-p) NDI@SWNT composite dispersion (in 1:99% DMSO:EMEM) containing 21 μg/mL NDI anchored onto 35 μg/mL SWNT: DIC (m), DIC-green-red channels overlay (n), green channel (515-530 nm) (o) and red channel (605-675 nm) (p). Scalebar 20 μm. The cells shown in figures i-l and m-p below are exactly the same as those shown in Figure 10 (below) images (d)–(e) and (f)–(g) respectively.

onto SWNTs (whereby the mass ratio of NDI:SWNT was kept at 0.6, consistent with observations from fluorescence titrations) and concentrations ranging from 1 μg/mL to 250 μg/mL for the pristine SWNT. MI_{50} values were estimated in each case from five repeat experiments (see Supplementary Information). It was interesting to note that after 24 h incubation at 37 °C the pristine SWNTs seem to be significantly more cytotoxic than the NDI-functionalised SWNTs. MI_{50} values for free and functionalized SWNTs are within the same order of magnitude with earlier reports of the uptake of functionalised carbon nanotubes in vitro.[8,33,62,64,93,94] Confocal imaging experiments already showed that both free NDI and NDI@SWNTs localise in the cell cytoplasm and partially in the nucleus too. Interestingly, an inspection of the cell morphology of free NDI treated cells suggested that these are significantly more damaged than of those treated with the NDI@SWNT composite or free NDI within 2 h incubation time. MTT assays suggest that NDI@SWNTs has a somewhat lower cytotoxicity compared to that of the free SWNTs and free NDI healthy cells (FEK-4) versus in cancerous (MCF-7). Interestingly, MI_{50} data estimated by MTT assays over the traditional 24 h observation period showed significantly lower toxicity of NDI@SWNT towards FEK4 when compared to MCF-7. Cell viability tests support the hypothesis from imaging experiments that that free NDI, NDI@SWNT and free SWNTs all act upon healthy (FEK-4) and cancerous cells within 2-24 h (**Figure 11**) over a wide range of concentrations, but that the NDI modulates the biocompatibility of the SWNTs and the resulting composite localises in the cell cytoplasm as an intact object. The NDI@SWNT composite has a higher cytotoxicity to cancer cells MCF-7 than to normal cells FEK-4, as shown both by MI_{50} determinations (**Table 2**, Figure 11 and Supplementary Materials, Figure S16) and via time-lapse MTT experiments (Supplementary Information). Both free NDI and SWNT-supported NDI (NDI@SWNT) exhibit low toxicity up to 6 h incubation in FEK-4 cells, with cell viability higher than 89% and 96% respectively. After 24 h incubation with NDI and NDI@SWNT, FEK-4 cells showed lower viability by comparison to that of controls, of 25% and 45% respectively. Cell viability for the group treated with NDI@SWNT was 5% higher than for the case when free SWNTs were used, suggesting an increase of the SWNT biocompatibility upon wrapping and the significantly altered behavior of NDI@SWNT composite in vitro with respect to its individual components, i.e., free NDI or SWNT. In MCF-7 cells, free NDI as well as SWNT-supported NDI showed notable cytotoxicity at shorter time points. Cells treated with the NDI@SWNT composite show 53% viability after 6 h incubation for MCF-7 versus 96% observed for FEK-4. Pristine SWNTs showed cytotoxicity after 1–3 h incubation for both cell lines, with the faster inhibition observed in FEK-4 cells. The cell viability after 6 h incubation with NDI@SWNT was higher than that of pristine SWNT (96% *vs* 63%, see Figure S17, Supplementary Information). Further investigations are underway in our laboratories to fully establish the precise mechanism for these differences, and whether size and/or shape of this new nanoparticle are influencing the biolocalisation and ultimately their toxicity in vivo.[34,94–98]

We observed that the surface functionalization of carbon nanotubes with NDI reduces the SWNT toxicity behavior significantly both in cancerous and non-cancerous cell lines and mediates the biocompatibility of pristine SWNTs. Supramolecular wrapping is rapid and uniform thus bypassing the need for complex covalent synthetic procedures to be performed directly on the SWNT surface.[99–101] The new NDI reported hereby is a biocompatible nanoreceptor that may be derivatized further by virtue of the carboxylic groups: our method of SWNTs wrapping will facilitate the rapid incorporation of targeting peptides onto

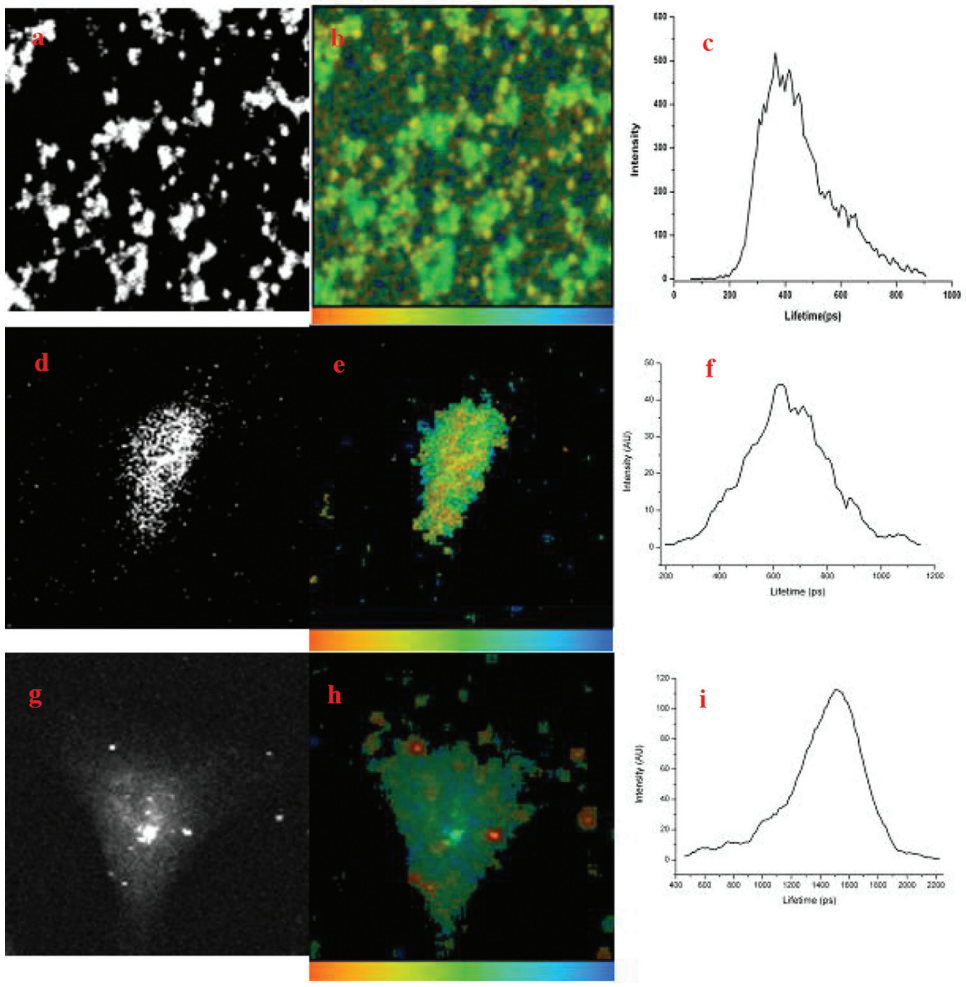

Figure 10. Two-photon laser confocal fluorescence (λ_{ex} = 910 nm): a–c) solid NDI@SWNT composite (drop-cast on borosilicate glass from a $CHCl_3$:EtOH 4:1 mixture): intensity image (a), lifetime mapping and scalebar (b) and corresponding lifetime distribution curve (c); d–f) Typical microscopy image of adherent cancerous cells (HeLa) incubated for 2 h at 37 °C with NDI (26 µM or 21 µg/mL in 1: 99% DMSO EMEM) showing NDI uptake throughout cytoplasm and cell nucleus, intensity image (d), lifetime mapping and scalebar (e) and corresponding lifetime distribution curve (f); g–i) Typical microscopy images of adherent cancerous cells (HeLa) incubated for 2 h at 37 °C with NDI@SWNT composite (dispersions in 1: 99% DMSO: EMEM contained 21 µg/mL NDI (26 µM) "anchored" onto 35 µg/mL SWNT. Intensity image (g), lifetime mapping and scalebar (h), and corresponding lifetime distribution curve (i). Bright spots show fluorescent NDI@SWNT composites translocated into cells as intact objects: corresponding single photon confocal fluorescence microscopy images and DICs are given in Supplementary materials (Scalebar/ microscopy images width = 100 µm. A key is provided for direct correlation between the lifetime colour map and lifetime histogram. The cells shown in figures (d)–(e) and (f)–(g) below are the same as those in Figure 9, images (i)–(l) and (m)–(p) respectively.

the surface of SWNTs for precise cancer cell delivery in vitro. Experiments are underway in our laboratories to construct and test in vitro and in vivo future nanotherapeutics based on this optically traceable NDI@SWNT scaffold.

3. Conclusions

In summary, we have developed a rapid and reliable method for the surface functionalization of SWNTs via encapsulation by a new nanoreceptor, NDI, which acts as a supramolecular host. A new supramolecularly-functionalized fluorescent nanomaterial was synthesized on a preparative scale. Iodine atoms featured as a key design motif in the NDI structure to aid the identification by TEM of the uniform coating of the surface of the carbon nanotubes.[3,101] The "host" is tightly wrapped around the carbon nanotube, forming a monolayer of NDI held to the aromatic surface by π–π stacking reinforced by solvophobic effects. The NDI network adapts its geometry in order to accommodate a guest with diameters as wide as 1.6 nm (i.e., a [10,10] SWNT). Charge transfer interactions are likely to occur between host (NDI) and guest (SWNT) in these composites in dispersions as suggested by significant quenching in fluorescence emission and DFT calculations in the gas phase.

The NDI@SWNT hybrid is biocompatible, translocates in cells as an intact object and shows fluorescence emission in the visible range. Confocal fluorescence imaging showed that

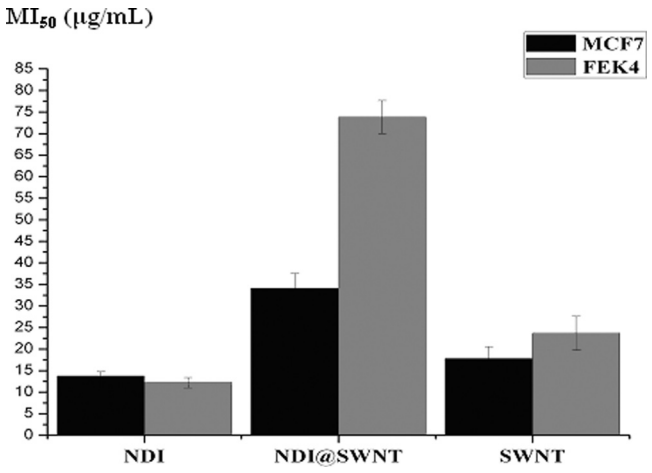

Figure 11. A comparison of MI50 values (μg/mL) for free NDI, NDI@ SWNT and free SWNT in healthy (FEK-4) and cancerous cells (MCF-7). Cells were cultured in EMEM containing the standard% FCS required for each of the cell lines used, each experiment was repeated five times.

Table 2. Calculated MI_{50} (± SEM values, μg/mL, the concentration that reduces cell metabolism to half that of untreated cells, 24 h MTT assay) for free NDI, NDI@ SWNT and free SWNT. Cells were cultured in EMEM containing 15% FCS, each experiment was repeated five times.

MI_{50} μg/mL	MCF-7 Breast carcinoma	FEK-4 Normal human fibroblast cell line
NDI	13.76 ± 1.00	12.21 ± 1.17
NDI@SWNT	34.08 ± 3.46	73.79 ± 3.87
SWNT	17.81 ± 2.71	23.66 ± 3.90

localization in sub-cellular (FEK-4 and MCF-7) regions and that the NDI coating significantly enhances the biocompatibility of SWNTs and mediates its intracellular localization. The excited state lifetime of the probes in cells versus solution phase indicates that the probes are not affected by the change in their chemical environment. The new amino acid functionalized NDI is amenable for further rapid derivatization with functional groups and/or biomolecules[92] *via* simple peptide coupling chemistry. Supramolecular coating led to the controlled and uniform functionalization of the whole of SWNTs surface, including the coating of the SWNTs ends in a manner analogous to the fullerene binding by similar NDI-based nanoreceptors and without the disruption of the aromatic network. This new nanohybrid showed a significant output in the visible spectrum, opening up future possibilities for its incorporation in the next generation optoelectronic devices for both photovoltaic and biomedical imaging applications. We are now investigating further amino acid- and targeting peptide-derivatized NDI molecules as key components for the rapid assembly of imaging and drug delivery devices based on carbon nanomaterials.

4. Experimental Section

*Synthesis of NDI ((2S,2'S)-2,2'-(1,3,6,8-tetraoxobenzo[lmn][3,8] phenanthroline-2,7(1H,3H,6H,8H)-diyl)bis(3-(4-iodophenyl)propanoic acid)) (**Scheme 1**)*:1,4,5,8-Naphthalenetetracarboxylic dianhydride (200 mg, 0.746 mmol) and 4-iodophenylalanine (4.34 mg, 1.492 mmol) were suspended in 6 mL DMF in a pressure tight 8 mL microwave vial. To this suspension 0.2 mL dry Et_3N were added. The suspension was sonicated until the mixture became homogenous. The reaction mixture was heated for 5 min at 140 °C under microwave irradiation using a dedicated microwave reactor (CEM Discover). The solvent was removed under reduced pressure. The dark brown residue was taken up into CH_3CN (4 mL). This solution was added under stirring to 100 mL of 1M HCl. The resulting suspension was allowed to settle for 1 hour and then filtered using a Büchner funnel. The solid was then washed with 150 mL deionized water and dried in vacuo. The product was obtained in the form of a pale yellow solid in 87% yield.

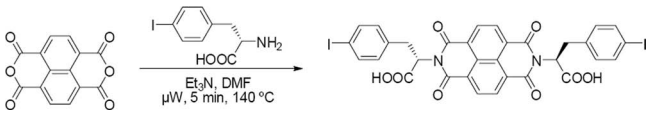

Scheme 1. Synthesis of iodine-derivatized NDI.

^{1}H NMR (400 MHz, 1:1 $CDCl_3$:CD_3OD) δ(ppm): 8.63 (s, 4H, NDI-CH), 7.40 (d, J = 8.3, 4H, Ph-CH), 5.95 (dd, J_1 = 10.4, J_2 = 5.5, 2H, $C^{\alpha}H$), 3.61 (dd, J_1 = 14.4, J_2 = 5.5, 2H, $C^{\beta}H$), 3.45 (dd, J_1 = 14.4, J_2 = 10.4, 2H, $C^{\beta}H$); ^{13}C {^{1}H}NMR (100.61 MHz, DMSO-d_6) δ(ppm): 171.5, 163.1, 137.9, 137.4, 131.8, 131.6, 127.3, 126.8, 92.5, 55.0, 34.8. Mass spectrometry: Negative mode ES: M/z calcd: $C_{32}H_{20}I_2N_2O_8$ 813.9309 found: 813.9251 [M^-].

Crystal Structure Dtermination: Single crystal X-ray diffraction data was obtained for NDI. Crystals suitable for analysis were grown from THF layered with pentane. A typical crystal was mounted using the oil drop technique, in perfluoropolyether oil at 150(2) K with a Cryostream N_2 open-flow cooling device. Single crystal X-ray diffraction data were collected using graphite monochromated Mo-Kα radiation (λ = 0.71073 Å) on an Nonius KappaCCD diffractometer.[102,103] The structures were solved by direct methods by using the program SHELXL97.[104] The refinement (on F^2) and graphical calculations were performed with the SHELXL97.[105] In general, coordinates and anisotropic displacement parameters of all non-hydrogen atoms were refined except where this was not possible due to the presence of disorder. The structure shows nanotubular channels which are filled with disordered solvent molecules (Figure 1). Abbreviated crystal data and structure refinement parameters are included in below.

NDI •2THF: C_{40} H_{36} I_2 N_2 O_{10}: M = 814.319, Z = 2, monoclinic P_{21} space group a = 12.7594(4)Å, b = 9.2119(3)Å, c = 16.3278(6)Å, β = 103.4340(10)°, U = 1866.63(11)Å^3, T = 150 (2) K, μ = 1.747 mm^{-1}, λ = 0.71073 Å. Of 28017 reflections measured, 8439 were independent (Rint = 0.0953). Final R = 0.0486 (6146 reflections with I > 2σ (I)) and wR = 0.0812.

Crystallographic data (excluding structure factors) for the structure reported in this paper have been deposited with the Cambridge Crystallographic Data Centre as supplementary publication no. CCDC-.736937. Data can be obtained free of charge from The Cambridge Crystallographic Data Centre via www.ccdc.cam.ac.uk/data_request/cif.

Cells Clturing (FEK-4, MCF-7 and HeLa) and Fuorescence Imaging: Cells were cultured at 37 °C in a humidified atmosphere of 5% CO_2 in air and split once confluence had been reached, using EMEM medium (Eagle's Modified Essential Medium) with 15% foetal calf serum (FCS), (10% for HeLa and MCF-7 and 15% for FEK-4), 200 U mL^{-1} L-glutamine and 100 U mL^{-1} penicillin. The medium contained no fluorescent indicator dyes such as phenol red and was therefore suitable for use in fluorescence imaging studies. Samples for fluorescence imaging were prepared in the following way: surplus supernatant after culturing (containing dead cell matter and excess proteins) was discarded. The live adherent cells were then washed with two 5 mL aliquots of phosphate buffer saline solution to remove any remaining medium containing FCS since this contains protease inhibitors which inactivate trypsin, thus inhibiting the resuspension of the cells. For re-suspension in solution, the cells were incubated in 3 mL of trypsin–EDTA (500 mg L^{-1} trypsin, 200 mg L^{-1}

EDTA) solution for 5 min at 37 °C. After trypsinizing, fresh EMEM (15% FCS) was added to the suspended cells to give a sufficient concentration of cells (ca. 50 000 cells/mL). The concentration of cells required varied slightly between cell lines and is chosen to be optimal for achieving sufficient coverage on the Petri dish for optimal imaging (between 40–60% coverage). The cells were plated in a Petri dish with a glass cover slip (Mattek) and left for 24 h to adhere before fluorescence imaging measurements were made. Final concentrations on cell plates used, in 1: 99 DMSO: EMEM, were: a) 21 μg/ml (26 μM) NDI; b) NDI@SWNT composite dispersion containing 21 μg/mL NDI (26 μM solution used to 'anchor' NDI onto 35 μg/mL SWNT); c) 35 μg/mL dispersion of free SWNT. Cells were incubated for maximum 2h followed by washing prior to imaging. Cell viability prior to the experiment was tested by optical microscopy, standard trypan blue tests and MTT assays. The uptake of the NDI@SWNT composite was imaged by laser-scanning confocal microscopy (LSM 510 META, Zeiss) of live cells, as well as in fixed cells, using the 488 nm line of an argon ion laser for excitation. The emission was long pass filtered (515 nm) and detected with a photomultiplier tube (PMT). The intensity of the laser was modified to reduce the possibility of photobleaching of the fluorophore over time and the PMT voltage adjusted to be just above the auto-fluorescence limit of the starting conditions (for imaging of living cells) thus recording a background image before addition of compound, whilst maximizing sensitivity and ensuring optimal focusing. A similar standard procedure was used for imaging fixed cells, and for these an additional background image was collected (using fixed, but untreated cells) at the end of experiment. The confocal imaging of the cells using λ_{ex} 405 nm did not show significant fluorescence emission for either free NDI or NDI@SWNTs thus allowing colocalization tests with nuclear staining dyes such as Hoechst or DAPI (Invitrogen). A strong fluorescence emission was observed in the green (515–530 nm) and red (605–675 nm) channels upon single-photon laser confocal microscopy using excitation with a green laser (488 nm). Upon incubation with the NDI@SWNT probe, formation of endosomes of ca. 0.5–1 μm seems to be suggested by both bright field and fluorescence imaging inside the cells' cytoplasm. The largest of NDI@SWNT aggregates (ca. 4 μm) did not appear to cross the outer membrane and remained attached to the outside membrane of the cell. After exposure to NDI@SWNT the cell membrane did not show any significant disruption or changes in morphology within 1 h incubation time at 37 °C. In contrast, when the experiment was repeated using either free NDI or pristine SWNT imaging showed that these distributed rapidly both inside the cells throughout the cytoplasm and in the nucleus and visibly altered the cell membrane morphology within 1 h of incubation.

In Vitro Fluorescence Lifetime Imaging (FLIM): Time correlated single photon counting (TCSPC) and FLIM data was performed using a two-photon microscope at the Central Laser Facility of the Rutherford Appleton Laboratory with some modifications. Briefly, a two-photon microscope was constructed around a Nikon TE2000-U inverted microscope using custom-made XY galvanometers (GSI Lumonics) for the scanning system. Tunable laser light at the required wavelength of 910 nm was obtained from a mode-locked titanium sapphire laser (Mira; Coherent Lasers), producing 180-fs pulses at 75 MHz, pumped by a solid-state continuous wave 532-nm laser (Verdi V18; Coherent Laser). The oscillator fundamental output of 910 ± 2 nm was also used. The laser beam was focused to a diffraction limited spot through a water immersion ultraviolet corrected objective (Nikon VC ×60, numeric aperture 1.2) and specimens illuminated at the microscope stage of a modified Nikon TE2000-U with UV transmitting optics. The focused laser spot was raster scanned using an X-Y galvanometer (GSI Lumonics). Fluorescence emission was collected without de-scanning, bypassing the scanning system and passed through a coloured glass (BG39) filter. The scan was operated in normal mode and line, frame and pixel clock signals were 20 generated and synchronized with an external fast microchannel plate photomultiplier tube used as the detector (R3809-U, Hamamatsu, Japan). These were linked via a time-correlated single-photon-counting PC module SPC830 (Becker and Hickl) to generate the multiphoton excited image with the associated characteristic decay at each pixel position. The decays were subsequently analyzed to generate the FLIM image. Prior to 2 photon FLIM data collection, the probe loaded cells were confirmed using a Nikon eC1 confocal microscope with excitation at 405nm, 488 and 543 nm where required. Data were analyzed using the SPCImage analysis software (Becker and Hickl). The $\chi 2$ value 2 between 0.9 and 1.3 were taken to represent a good fitting curve and where necessary, the decay profiles were fitted with two, rather than one exponential. The distribution of lifetime values within the ROI were generated and displayed as a FLIM image.

Cell Viability Tests in FEK-4 and MCF-7 Cell lines by MTT Assays: Cell viability studies were carried out under conditions closely comparable with the imaging experiments. Stock solutions were prepared as follows: samples containing 42 μg NDI, 42 μg NDI anchored onto 70 μg SWNT (mass ratio NDI:SWNT = 0.6) and 70 μg purified SWNT were each treated with 2 mL $CHCl_3$: EtOH (4:1) and sonicated for ca 20 min. After sonication, the solvent was completely removed and 100 μL DMSO was added to each of the residues, followed by further sonication for ca 20 min. Aliquots from each of the stock solutions were added to EMEM and immediately added to the wells containing cells ready for treatment such that the final DMSO content in EMEM was 1%. The final concentration of the probes added to each well was: a) 42 μg free NDI, b) NDI@SWNT composite, formed by anchoring 42 μg NDI onto 70 μg SWNT and c) 70 μg SWNT, each dispersed in 100 μL solvent (1: 99 DMSO: EMEM). Two control groups were used consisting of 100 μL solvent/well, i.e 1%: 99% EMEM, as well as 100% EMEM. FEK-4 and MCF-7 cell lines (cultured using standard procedures[106]) were incubated at 37 °C with the samples prepared as above for 1 h, 3 h, 6 h and 24 h. After incubation, wells were aspirated and solvents replaced by 100 μL of 0.5 mg/mL MTT (3-(4,5-dimethylthiazol-2-yl)-2,5-diphenyltetrazolium bromide) in EMEM:PBS 9:1, followed by a further incubation (at 37 °C) for 2 h.[107,108] The MTT solution was then aspirated and 100 μL of DMSO was added. Absorbance of resulting samples (directly proportional to cell viability) was measured at 570 nm using a plate reader. Cell viability (%) was estimated as [experiment group OD value] x 100/[control group OD value].

Further details can be found in the Supporting Information: (1) Additional TEM and HRTEM microscopy images, (2) solid state FT IR, (3) Fluorescence spectroscopy additional data, (4) Circular dichroism, (5) UV–vis spectroscopy (6) Reference configuration and cut-off radii (a.u.) of the pseudopotentials used in the DFT modeling study and a comparison with simpler NDI@C60 models (7) Conditions of FEK-4 and MCF-7 cells culturing, fluorescence imaging and additional confocal and epifluorescence imaging in FEK-4 and MCF-7 (8) Time-lapse assay by MTT assays following cells viability under conditions comparable to those of the imaging experiment. (9) FLIM and corresponding confocal fluorescence imaging including lysotracker and mitotracker co-localization tests in MCF-7 lines.

Supporting Information

Supporting Information is available from the Wiley Online Library or from the author.

Acknowledgements

Professor Malcolm L.H. Green FRS and the Oxford Nanotube Group are acknowledged for helpful discussions and training in handling SWNTs and Thomas Swann Ltd. and Dr Davide Mattia (Bath University) for assistance with the provision and the advanced purification of the Elicarb SWNTs used hereby. Colin Wright (Nikon Bioimaging UK Ltd), Julia Zhong (Bath Pharmacology) and Alison Crossley (Begbroke Nano) are thanked for training and experimental support. We are grateful to the Research Complex at Harwell and Nikon Bioimaging UK for providing access to fluorescence imaging equipment. The Royal Society (SIP), MRC (SIP), STFC (SIP), University of Bath (SIP, GDP, ZH, RLA), EPSRC (JKMS) and Pembroke College, Cambridge (GDP) are thanked for financial support.

The authors thank EPSRC National Service for Computational Chemistry Software for training, support and computational facilities and EPSRC Mass Spectrometry facility at Swansea for assistance.

Received: August 17, 2011
Published online: December 8, 2011

[1] D. Guldi, *Phys. Chem. Chem. Phys.* **2007**, *9*, 1400.
[2] D. M. Guldi, G. M. A. Rahman, V. Sgobba, C. Ehli, *Chem. Soc. Rev.* **2006**, *35*, 471.
[3] A. A. Eliseev, M. V. Chernysheva, N. I. Verbitskii, E. A. Kiseleva, A. V. Lukashin, Y. D. Tretyakov, N. A. Kiselev, O. M. Zhigalina, R. M. Zakalyukin, A. L. Vasiliev, A. V. Krestinin, J. L. Hutchison, B. Freitag, *Chem. Mater.* **2009**, *21*, 5001.
[4] H. Ali-Boucetta, K. T. Al-Jamal, D. McCarthy, M. Prato, A. Bianco, K. Kostarelos, *Chem. Commun.* **2008**, 459.
[5] R. J. Chen, S. Bangsaruntip, K. A. Drouvalakis, N. W. S. Kam, M. Shim, Y. M. Li, W. Kim, P. J. Utz, H. J. Dai, *Proc. Nat. Acad. Sci. USA* **2003**, *100*, 4984.
[6] J. H. Choi, F. T. Nguyen, P. W. Barone, D. A. Heller, A. E. Moll, D. Patel, S. A. Boppart, M. S. Strano, *Nano Lett.* **2007**, *7*, 861.
[7] S. Dhar, Z. Liu, J. Thomale, H. J. Dai, S. J. Lippard, *J. Am. Chem. Soc.* **2008**, *130*, 11467.
[8] D. A. Heller, S. Baik, T. E. Eurell, M. S. Strano, *Adv. Mat.* **2005**, *17*, 2793.
[9] K. Balasubramanian, R. Sordan, M. Burghard, K. Kern, *Nano Lett.* **2004**, *4*, 827.
[10] M. A. Loi, J. Gao, F. Cordella, P. Blondeau, E. Menna, B. Bartova, C. Hebert, S. Lazar, G. A. Botton, M. Milko, C. Ambrosch-Draxl, *Adv. Mater.* **2010**, *22*, 1635.
[11] S. I. Pascu, N. Kuganathan, L. H. Tong, R. M. J. Jacobs, P. J. Barnard, B. T. Chu, Y. Huh, G. Tobias, C. G. Salzmann, J. K. M. Sanders, M. L. H. Green, J. C. Green, *J. Mat. Chem.* **2008**, *18*, 2781.
[12] C. Backes, F. Hauke, C. D. Schmidt, A. Hirsch, *Chem. Commun.* **2009**, 2643.
[13] C. Backes, C. D. Schmidt, F. Hauke, C. Boettcher, A. Hirsch, *J. Am. Chem. Soc.* **2009**, *131*, 2172.
[14] C. Oelsner, C. Schmidt, F. Hauke, M. Prato, A. Hirsch, D. M. Guldi, *J Am Chem Soc* **2011**, *133*, 4580.
[15] M. S. Arnold, M. O. Guler, M. C. Hersam, S. I. Stupp, *Langmuir* **2005**, *21*, 4705.
[16] K. Balasubramanian, M. Friedrich, C. Y. Jiang, Y. W. Fan, A. Mews, M. Burghard, K. Kern, *Adv. Mat.* **2003**, *15*, 1515.
[17] M. K. Bayazit, K. S. Coleman, *J. Am. Chem. Soc.* **2009**, *131*, 10670.
[18] J. Y. Chen, C. P. Collier, *J. Phys. Chem. B* **2005**, *109*, 7605.
[19] P. Cherukuri, C. J. Gannon, T. K. Leeuw, H. K. Schmidt, R. E. Smalley, S. A. Curley, R. B. Weisman, *Proc. Nat. Acad. Sci. USA* **2006**, *103*, 18882.
[20] M. De, P. S. Ghosh, V. M. Rotello, *Adv. Mat.* **2008**, *20*, 4225.
[21] V. V. Didenko, V. C. Moore, D. S. Baskin, R. E. Smalley, *Nano Lett.* **2005**, *5*, 1563.
[22] H. Jin, D. A. Heller, M. S. Strano, *Nano Lett.* **2008**, *8*, 1577.
[23] Y. Lee, K. E. Geckeler, *Adv. Mater.* **2010**, *22*, 4076.
[24] Z. Liu, K. Chen, C. Davis, S. Sherlock, Q. Z. Cao, X. Y. Chen, H. J. Dai, *Cancer Res.* **2008**, *68*, 6652.
[25] Z. Liu, A. C. Fan, K. Rakhra, S. Sherlock, A. Goodwin, X. Y. Chen, Q. W. Yang, D. W. Felsher, H. J. Dai, *Angew. Chem.-Int. Ed.* **2009**, *48*, 7668.
[26] M. A. Loi, J. Gao, F. Cordella, P. Blondeau, E. Menna, B. Bartova, C. Hebert, S. Lazar, G. A. Botton, M. Milko, C. Ambrosch-Draxl, *Adv. Mater.* **2010**, *22*, 1635.
[27] H. Murakami, T. Nomura, N. Nakashima, *Chem. Phys. Lett.* **2003**, *378*, 481.
[28] N. Nakayama-Ratchford, S. Bangsaruntip, X. Sun, K. Welsher, H. Dai, *J. Am. Chem. Soc.* **2007**, *129*, 2448.
[29] M. J. O'Connell, S. M. Bachilo, C. B. Huffman, V. C. Moore, M. S. Strano, E. H. Haroz, K. L. Rialon, P. J. Boul, W. H. Noon, C. Kittrell, J. P. Ma, R. H. Hauge, R. B. Weisman, R. E. Smalley, *Science* **2002**, *297*, 593.
[30] Z. M. Ou, B. Y. Wu, D. Xing, F. F. Zhou, H. Y. Wang, Y. H. Tang, *Nanotechnology* **2009**, *20*.
[31] S. Tamesue, M. Numata, K. Kaneko, T. D. James, S. Shinkai, *Chem. Commun.* **2008**, 4478.
[32] K. Welsher, Z. Liu, D. Daranciang, H. Dai, *Nano Letters* **2008**, *8*, 586.
[33] W. R. Yang, P. Thordarson, J. J. Gooding, S. P. Ringer, F. Braet, *Nanotechnology* **2007**, *18*.
[34] C. Zavaleta, A. de la Zerda, Z. Liu, S. Keren, Z. Cheng, M. Schipper, X. Chen, H. Dai, S. S. Gambhir, *Nano Lett.* **2008**, *8*, 2800.
[35] W. H. Zhu, N. Minami, S. Kazaoui, Y. Kim, *J. Mater. Chem.* **2003**, *13*, 2196.
[36] S. Z. Zu, X. X. Sun, Y. Q. Liu, B. H. Han, *Chem. Asian J.* **2009**, *4*, 1562.
[37] G. D. Pantoş, P. Pengo, J. K. M. Sanders, *Angew. Chem.-Int. Ed.* **2007**, *46*, 194.
[38] T. D. M. Bell, S. Yap, C. Jani, S. J. Langford, J. Hofkens, F. De Schryver, K. P. Ghiggino, *Proceedings SPIE-The International Society of Optical Engineering* **2007**, *6444*, 644404.
[39] S. Bevers, T. P. O'Dea, L. W. McLaughlin, *J. Am. Chem. Soc.* **1998**, *120*, 11004.
[40] S. V. Bhosale, C. H. Jani, S. J. Langford, *Chem.Soc. Rev.* **2008**, *37*, 331.
[41] M. F. Brana, J. M. Castellano, M. Moran, M. J. P. Devega, C. R. Romerdahl, X. D. Qian, P. Bousquet, F. Emling, E. Schlick, G. Keilhauer, *Anti-Cancer Drug Design* **1993**, *8*, 257.
[42] D. A. Gianolio, L. W. McLaughlin, *Bioorg. Med. Chem.* **2001**, *9*, 2329.
[43] S. Matsugo, S. Kawanishi, K. Yamamoto, H. Sugiyama, T. Matsuura, I. Saito, *Angew. Chem-Int. Ed.* **1991**, *30*, 1351.
[44] T. B. Singh, S. Erten, S. Gunes, C. Zafer, G. Turkmen, B. Kuban, Y. Teoman, N. S. Sariciftci, S. Icli, *Organic Electronics* **2006**, *7*, 480.
[45] E. Tamanini, N. Ponnuswamy, G. D. Pantoş, J. K. M. Sanders, *Faraday Discuss.* **2009**, *145*, 205.
[46] V. Guelev, S. Sorey, D. W. Hoffman, B. L. Iverson, *J. Am. Chem. Soc.* **2002**, *124*, 2864.
[47] R. S. Lokey, Y. Kwok, V. Guelev, C. J. Pursell, L. H. Hurley, B. L. Iverson, *J. Am. Chem. Soc.* **1997**, *119*, 7202.
[48] R. J. Abdel-Jalil, M. Aqarbeh, D. Loffler, B. Shen, S. A. Orabi, W. Voelter, H. J. Machulla, *J. Radioanal. Nucl. Chem.* **2010**, *283*, 239.
[49] C. J. Koch, S. M. Evans, in "*Oxygen Transport to Tissue XXIII*", ed. D. Wilson, Kluver Academic/Plenum Publishers, **2003**, *510*, 285.
[50] F. Riche, A. D. d'Hardemare, S. Sepe, L. Riou, D. Fagret, M. Vidal, *Bioorg. Med. Chem. Lett.* **2001**, *11*, 71.
[51] N. Ashkenasy, W. S. Horne, M. R. Ghadiri, *Small* **2006**, *2*, 99.
[52] Y. Chu, S. Sorey, D. W. Hoffman, B. L. Iverson, *J. Am. Chem. Soc.* **2007**, *129*, 1304.
[53] R. Martinez, L. Chacon-Garcia, *Curr. Med. Chem.* **2005**, *12*, 127.
[54] K. Tambara, N. Ponnuswamy, G. Hennrich, G. D. Pantoş, *J. Org. Chem.* **2011**, *76*, 3338–3347.
[55] P. Pengo, G. D. Pantoş, S. Otto, J. K. Sanders, *J Org Chem* **2006**, *71*, 7063.
[56] E. Tamanini, G. D. Pantoş, J. K. Sanders, *Chem.-Eur. J.* **2010**, *16*, 81.
[57] A. R. Stefankiewcz, E. Tamanini, G. D. Pantoş, J. K. M. Sanders, *Angew. Chem., -Int. Ed.* **2011**, *50*, 5725–5728.
[58] J. L. Wietor, G. D. Pantoş, J. K. M. Sanders, *Angew. Chem.-Int. Ed.* **2008**, *47*, 2689.
[59] N. Ponnuswamy, G. D. Pantoş, J. K. Sanders, *Faraday Discuss.* **2009**, *145*, 205.

[60] B. M. Bulheller, G. D. Pantoş, J. K. M. Sanders, J. D. Hirst, *Phys. Chem. Chem. Phys.* **2009**, *11*, 6060.
[61] A. Bianco, K. Kostarelos, M. Prato, *Exp. Op. Drug Deliv.* **2008**, *5*, 331.
[62] M. Bottini, S. Bruckner, K. Nika, N. Bottini, S. Bellucci, A. Magrini, A. Bergamaschi, T. Mustelin, *Toxicol. Lett.* **2006**, *160*, 121.
[63] M. Bottini, F. Cerignoli, M. I. Dawson, A. Magrini, N. Rosato, T. Mustelin, *Biomacromolec.* **2006**, *7*, 2259.
[64] D. X. Cui, F. R. Tian, C. S. Ozkan, M. Wang, H. J. Gao, *Toxicol. Lett.* **2005**, *155*, 73.
[65] P. Kubat, K. Lang, P. Janda, O. Frank, I. Matulkova, J. Sykora, S. Civis, M. Hof, L. Kavan, *J. Nanosci. Nanotechnol.* **2009**, *9*, 5795.
[66] S. J. Lin, G. Keskar, Y. N. Wu, X. Wang, A. S. Mount, S. J. Klaine, J. M. Moore, A. M. Rao, P. C. Ke, *Appl. Phys. Lett.* **2006**, *89*.
[67] S. I. Pascu, R. L. Arrowsmith, S. R. Bayly, S. Brayshaw, Z. Hu, *Phil Trans R. Soc. A 2010*, **1924**, *368*, 3683.
[68] A. E. Porter, M. Gass, K. Muller, J. N. Skepper, P. A. Midgley, M. Welland, *Nat. Nanotechnol.* **2007**, *2*, 713.
[69] K. Konig, *J. Microsc.* **2000**, *200*, 83.
[70] K. Suhling, P. M. W. French, D. Phillips, *Photochem. Photobiol. Sci.* **2005**, *4*, 13.
[71] G. E. Stutzmann, I. Parker, *Physiology* **2005**, *20*, 15.
[72] M. Oheim, D. J. Michael, M. Geisbauer, D. Madsen, R. H. Chow, *Adv. Drug Delivery Rev.* **2006**, *58*, 788.
[73] R. H. Bisby, A. G. Crisostomo, S. W. Botchway, A. W. Parker, *Photochem. Photobiol.* **2009**, *85*, 353.
[74] S. W. Botchway, A. W. Parker, R. H. Bisby, A. G. Crisostomo, *Microsc. Res. Tech.* **2008**, *71*, 267.
[75] B. Treanor, P. M. P. Lanigan, K. Suhling, T. Schreiber, I. Munro, M. A. A. Neil, D. Phillips, D. M. Davis, P. M. W. French, *J. Microsc.* **2005**, *217*, 36.
[76] S. W. Botchway, M. Charnley, O. W. Haycock, A. W. Parker, D. L. Rochester, J. A. Weinstein, J. A. G. Williams, *Proc. Natl. Acad. Sci. U. S. A.* **2008**, *105*, 16071.
[77] E. Artacho, D. Sanchez-Portal, P. Ordejon, A. Garcia, J. M. Soler, *Phys. Status Solidi B* **1999**, *215*, 809.
[78] E. L. Sceats, J. C. Green, *J. Chem. Phys.* **2006**, *125*, 154704.
[79] P. Hobza, H. L. Selzle, E. W. Schlag, *J. Phys. Chem.* **1996**, *100*, 18790.
[80] M. S. Dresselhaus, A. Jorio, M. Hofmann, G. Dresselhaus, R. Saito, *Nano Lett.* **2010**, *10*, 751.
[81] C. G. Salzmann, B. T. T. Chu, G. Tobias, S. A. Llewellyn, M. L. H. Green, *Carbon* **2007**, *45*, 907.
[82] G. K. C. Lee, C. Sach, M. L. H. Green, L. L. Wong, C. G. Salzmann, *Chem. Commun.* **2010**, *46*, 7013.
[83] A. Ikeda, Y. Totsuka, K. Nobusawa, J. Kikuchi, *J. Mater. Chem.* **2009**, *19*, 5785.
[84] J. K. Sprafke, S. D. Stranks, J. H. Warner, R. J. Nicholas, H. L. Anderson, *Angew. Chem., Int. Ed.* **2011**, *50*, 2313.
[85] J. V. Caspar, T. J. Meyer, *J. Am. Chem. Soc.* **1983**, *105*, 5583.
[86] C. Thalacker, C. Roger, F. Wurthner, *J. Org. Chem.* **2006**, *71*, 8098.
[87] J. L. Wietor, G. D. Pantoş, J. K. M. Sanders, *Angew. Chem., Int. Ed.* **2008**, *47*, 2689.
[88] D. A. Heller, E. S. Jeng, T. K. Yeung, B. M. Martinez, A. E. Moll, J. B. Gastala, M. S. Strano, *Science* **2006**, *311*, 508.
[89] G. Dukovic, M. Balaz, P. Doak, N. D. Berova, M. Zheng, R. S. McLean, L. E. Brus, *J. Am. Chem. Soc.* **2006**, *128*, 9004.
[90] C. G. Salzmann, G. K. C. Lee, M. A. H. Ward, B. T. T. Chu, M. L. H. Green, *J. Mat. Chem.* **2008**, *18*, 1977.
[91] C. G. Salzmann, M. A. H. Ward, R. M. J. Jacobs, G. Tobias, M. L. H. Green, *J. Phys. Chem. C* **2007**, *111*, 18520.
[92] T. Nojima, K. Ohtsuka, T. Nagamatsu, S. Takenaka, *Nucleic Acids Res. Suppl.* **2003**, 123.
[93] H. Isobe, T. Tanaka, R. Maeda, E. Noiri, N. Solin, M. Yudasaka, S. Iijima, E. Nakamura, *Angew. Chem. Int. Ed.* **2006**, *45*, 6676.
[94] Y. L. Zhao, G. M. Xing, Z. F. Chai, *Nat. Nanotechnol.* **2008**, *3*, 191.
[95] M. R. McDevitt, D. Chattopadhyay, J. S. Jaggi, R. D. Finn, P. B. Zanzonico, C. Villa, D. Rey, J. Mendenhall, C. A. Batt, J. T. Njardarson, D. A. Scheinberg, *PLoS One* **2007**, *2*, e907.
[96] C. A. Poland, R. Duffin, I. Kinloch, A. Maynard, W. A. H. Wallace, A. Seaton, V. Stone, S. Brown, W. MacNee, K. Donaldson, *Nat. Nanotechnol.* **2008**, *3*, 423.
[97] H. F. Wang, J. Wang, X. Y. Deng, H. F. Sun, Z. J. Shi, Z. N. Gu, Y. F. Liu, Y. L. Zhao, *J. Nanosci. Nanotechnol.* **2004**, *4*, 1019.
[98] M. J. Welch, C. J. Hawker, K. L. Wooley, *J. Nucl. Med.* **2009**, *50*, 1743.
[99] K. Balasubramanian, M. Burghard, *Small* **2005**, *1*, 180.
[100] K. S. Coleman, S. R. Bailey, S. Fogden, M. L. H. Green, *J. Am. Chem. Soc.* **2003**, *125*, 8722.
[101] K. S. Coleman, A. K. Chakraborty, S. R. Bailey, J. Sloan, M. Alexander, *Chem. Mater.* **2007**, *19*, 1076.
[102] J. Cosier, A. M. Glazer, *J. Appl. Crystallogr.* **1986**, *19*, 105.
[103] Z. Otwinowski, W. Minor, *Methods Enzymol.* **1997**, *276*, 307.
[104] A. Altomare, G. Cascarano, C. Giacovazzo, A. Guagliardi, *J. Appl. Crystallogr.* **1993**, *26*, 343.
[105] G. M. Sheldrick, *Acta Crystallogr., Sect. A: Found. Crystallogr.* **2008**, *A64*, 112.
[106] S. I. Pascu, P. A. Waghorn, T. D. Conry, H. M. Betts, J. R. Dilworth, G. C. Churchill, T. Pokrovska, M. Christlieb, F. I. Aigbirhio, J. E. Warren, *Dalton Trans.* **2007**, 4988.
[107] T. Mosmann, *J. Immunol. Methods* **1983**, *65*, 55.
[108] S. F. Boys, F. Bernardi, *Mol. Phys.* **1970**, *19*, 553.